K^0_S production in τ decays

R. Barate, D. Buskulic, D. Decamp, P. Ghez, C. Goy, J P. Lees, A. Lucotte,
M N. Minard, J Y. Nief, B. Pietrzyk, et al.

K^0_S production in τ decays

The ALEPH Collaboration [1]

Abstract

From a sample of about 160k Z$\to\tau^+\tau^-$ candidates collected with the ALEPH detector at LEP between 1991 and 1995, τ lepton decays involving $K^0_S \to \pi^+\pi^-$ are studied. The $K^0_S K^0_L$ associated production in τ decays is also investigated. The branching ratios are measured for the inclusive decay $B(\tau^- \to K^0_S X^- \nu_\tau) = (9.70\pm0.58\pm0.62) \times 10^{-3}$, where X^- can be anything, and for the exclusive decays

$$
\begin{aligned}
B(\tau^-\to\overline{K}^0\pi^-\nu_\tau) &= (8.55\pm1.17\pm0.66) \times 10^{-3}, \\
B(\tau^-\to\overline{K}^0\pi^-\pi^0\nu_\tau) &= (2.94\pm0.73\pm0.37) \times 10^{-3}, \\
B(\tau^-\to\overline{K}^0 K^-\nu_\tau) &= (1.58\pm0.42\pm0.17) \times 10^{-3}, \\
B(\tau^-\to\overline{K}^0 K^-\pi^0\nu_\tau) &= (1.52\pm0.76\pm0.21) \times 10^{-3}.
\end{aligned}
$$

The decays $\tau^-\to K^0_S K^0_L \pi^-\nu_\tau$ is studied for the first time, giving a branching ratio

$$
B(\tau^-\to K^0_S K^0_L \pi^-\nu_\tau) = (1.01\pm0.23\pm0.13) \times 10^{-3}.
$$

The channels $\tau^- \to K^0_S K^0_S \pi^-\nu_\tau$, $\tau^- \to K^0_S K^0_S \pi^-\pi^0\nu_\tau$, $\tau^- \to K^0_S K^0_L \pi^-\pi^0\nu_\tau$, $\tau^-\to\overline{K}^0\pi^-\pi^0\pi^0\nu_\tau$, $\tau^-\to K^0 K^-\pi^0\pi^0\nu_\tau$ and $\tau^-\to K^0 h^+ h^- h^-\nu_\tau$ are also investigated. In addition, mass spectra in the $K^0_S h^-$ and $K^0_S h^-\pi^0$ final states are analysed to provide information on the intermediate states produced in the decays.

---

[1]See next pages for the list of authors.

The ALEPH Collaboration

R. Barate, D. Buskulic, D. Decamp, P. Ghez, C. Goy, J.-P. Lees, A. Lucotte, M.-N. Minard, J.-Y. Nief, B. Pietrzyk

Laboratoire de Physique des Particules (LAPP), IN^{2}P^3-CNRS, 74019 Annecy-le-Vieux Cedex, France

G. Boix, M.P. Casado, M. Chmeissani, J.M. Crespo, M. Delfino, E. Fernandez, M. Fernandez-Bosman, Ll. Garrido,[15] E. Graugès, A. Juste, M. Martinez, G. Merino, R. Miquel, Ll.M. Mir, I.C. Park, A. Pascual, J.A. Perlas, I. Riu, F. Sanchez

Institut de Física d'Altes Energies, Universitat Autònoma de Barcelona, 08193 Bellaterra (Barcelona), Spain[7]

A. Colaleo, D. Creanza, M. de Palma, G. Gelao, G. Iaselli, G. Maggi, M. Maggi, S. Nuzzo, A. Ranieri, G. Raso, F. Ruggieri, G. Selvaggi, L. Silvestris, P. Tempesta, A. Tricomi,[3] G. Zito

Dipartimento di Fisica, INFN Sezione di Bari, 70126 Bari, Italy

X. Huang, J. Lin, Q. Ouyang, T. Wang, Y. Xie, R. Xu, S. Xue, J. Zhang, L. Zhang, W. Zhao

Institute of High-Energy Physics, Academia Sinica, Beijing, The People's Republic of China[8]

D. Abbaneo, R. Alemany, U. Becker, P. Bright-Thomas, D. Casper, M. Cattaneo, F. Cerutti, V. Ciulli, G. Dissertori, H. Drevermann, R.W. Forty, M. Frank, R. Hagelberg, J.B. Hansen, J. Harvey, P. Janot, B. Jost, I. Lehraus, P. Mato, A. Minten, L. Moneta,[25] A. Pacheco, J.-F. Pusztaszeri,[23] F. Ranjard, L. Rolandi, D. Rousseau, D. Schlatter, M. Schmitt, O. Schneider, W. Tejessy, F. Teubert, I.R. Tomalin, H. Wachsmuth, A. Wagner[20]

European Laboratory for Particle Physics (CERN), 1211 Geneva 23, Switzerland

Z. Ajaltouni, F. Badaud, G. Chazelle, O. Deschamps, A. Falvard, C. Ferdi, P. Gay, C. Guicheney, P. Henrard, J. Jousset, B. Michel, S. Monteil, J-C. Montret, D. Pallin, P. Perret, F. Podlyski, J. Proriol, P. Rosnet

Laboratoire de Physique Corpusculaire, Université Blaise Pascal, IN^{2}P^3-CNRS, Clermont-Ferrand, 63177 Aubière, France

T. Fearnley, J.D. Hansen, J.R. Hansen, P.H. Hansen, B.S. Nilsson, B. Rensch, A. Wäänänen

Niels Bohr Institute, 2100 Copenhagen, Denmark[9]

G. Daskalakis, A. Kyriakis, C. Markou, E. Simopoulou, I. Siotis, A. Vayaki

Nuclear Research Center Demokritos (NRCD), Athens, Greece

A. Blondel, G. Bonneaud, J.-C. Brient, P. Bourdon, A. Rougé, M. Rumpf, A. Valassi,[6] M. Verderi, H. Videau

Laboratoire de Physique Nucléaire et des Hautes Energies, Ecole Polytechnique, IN^{2}P^3-CNRS, 91128 Palaiseau Cedex, France

T. Boccali, E. Focardi, G. Parrini, K. Zachariadou

Dipartimento di Fisica, Università di Firenze, INFN Sezione di Firenze, 50125 Firenze, Italy

M. Corden, C. Georgiopoulos, D.E. Jaffe

Supercomputer Computations Research Institute, Florida State University, Tallahassee, FL 32306-4052, USA [13,14]

A. Antonelli, G. Bencivenni, G. Bologna,[4] F. Bossi, P. Campana, G. Capon, V. Chiarella, G. Felici, P. Laurelli, G. Mannocchi,[5] F. Murtas, G.P. Murtas, L. Passalacqua, M. Pepe-Altarelli

Laboratori Nazionali dell'INFN (LNF-INFN), 00044 Frascati, Italy

L. Curtis, S.J. Dorris, A.W. Halley, J.G. Lynch, P. Negus, V. O'Shea, C. Raine, J.M. Scarr, K. Smith, P. Teixeira-Dias, A.S. Thompson, E. Thomson, F. Thomson

Department of Physics and Astronomy, University of Glasgow, Glasgow G12 8QQ,United Kingdom[10]

O. Buchmüller, S. Dhamotharan, C. Geweniger, G. Graefe, P. Hanke, G. Hansper, V. Hepp, E.E. Kluge, A. Putzer, J. Sommer, K. Tittel, S. Werner, M. Wunsch

Institut für Hochenergiephysik, Universität Heidelberg, 69120 Heidelberg, Fed. Rep. of Germany[16]

R. Beuselinck, D.M. Binnie, W. Cameron, P.J. Dornan, M. Girone, S. Goodsir, E.B. Martin, N. Marinelli, A. Moutoussi, J. Nash, J.K. Sedgbeer, P. Spagnolo, M.D. Williams

Department of Physics, Imperial College, London SW7 2BZ, United Kingdom[10]

V.M. Ghete, P. Girtler, E. Kneringer, D. Kuhn, G. Rudolph

Institut für Experimentalphysik, Universität Innsbruck, 6020 Innsbruck, Austria[18]

A.P. Betteridge, C.K. Bowdery, P.G. Buck, P. Colrain, G. Crawford, A.J. Finch, F. Foster, G. Hughes, R.W.L. Jones, M.I. Williams

Department of Physics, University of Lancaster, Lancaster LA1 4YB, United Kingdom[10]

I. Giehl, A.M. Greene, C. Hoffmann, K. Jakobs, K. Kleinknecht, G. Quast, B. Renk, E. Rohne, H.-G. Sander, P. van Gemmeren, C. Zeitnitz

Institut für Physik, Universität Mainz, 55099 Mainz, Fed. Rep. of Germany[16]

J.J. Aubert, C. Benchouk, A. Bonissent, G. Bujosa, J. Carr, P. Coyle, F. Etienne, O. Leroy, F. Motsch, P. Payre, M. Talby, A. Sadouki, M. Thulasidas, K. Trabelsi

Centre de Physique des Particules, Faculté des Sciences de Luminy, IN^2P^3-CNRS, 13288 Marseille, France

M. Aleppo, M. Antonelli, F. Ragusa

Dipartimento di Fisica, Università di Milano e INFN Sezione di Milano, 20133 Milano, Italy

R. Berlich, W. Blum, V. Büscher, H. Dietl, G. Ganis, C. Gotzhein, H. Kroha, G. Lütjens, G. Lutz, C. Mannert, W. Männer, H.-G. Moser, R. Richter, A. Rosado-Schlosser, S. Schael, R. Settles, H. Seywerd, H. Stenzel, W. Wiedenmann, G. Wolf

Max-Planck-Institut für Physik, Werner-Heisenberg-Institut, 80805 München, Fed. Rep. of Germany[16]

J. Boucrot, O. Callot,[2] S. Chen, Y. Choi,[21] A. Cordier, M. Davier, L. Duflot, J.-F. Grivaz, Ph. Heusse, A. Höcker, A. Jacholkowska, D.W. Kim,[12] F. Le Diberder, J. Lefrançois, A.-M. Lutz, I. Nikolic, M.-H. Schune, E. Tournefier, J.-J. Veillet, I. Videau, D. Zerwas

Laboratoire de l'Accélérateur Linéaire, Université de Paris-Sud, IN^2P^3-CNRS, 91405 Orsay Cedex, France

P. Azzurri, G. Bagliesi,[2] G. Batignani, S. Bettarini, C. Bozzi, G. Calderini, M. Carpinelli, M.A. Ciocci, R. Dell'Orso, R. Fantechi, I. Ferrante, L. Foà,[1] F. Forti, A. Giassi, M.A. Giorgi, A. Gregorio, F. Ligabue, A. Lusiani, P.S. Marrocchesi, A. Messineo, F. Palla, G. Rizzo, G. Sanguinetti, A. Sciabà, J. Steinberger, R. Tenchini, G. Tonelli,[19] C. Vannini, A. Venturi, P.G. Verdini

Dipartimento di Fisica dell'Università, INFN Sezione di Pisa, e Scuola Normale Superiore, 56010 Pisa, Italy

G.A. Blair, L.M. Bryant, J.T. Chambers, M.G. Green, T. Medcalf, P. Perrodo, J.A. Strong, J.H. von Wimmersperg-Toeller

Department of Physics, Royal Holloway & Bedford New College, University of London, Surrey TW20 OEX, United Kingdom[10]

D.R. Botterill, R.W. Clifft, T.R. Edgecock, S. Haywood, P.R. Norton, J.C. Thompson, A.E. Wright

Particle Physics Dept., Rutherford Appleton Laboratory, Chilton, Didcot, Oxon OX11 OQX, United Kingdom[10]

B. Bloch-Devaux, P. Colas, S. Emery, W. Kozanecki, E. Lançon, M.-C. Lemaire, E. Locci, P. Perez, J. Rander, J.-F. Renardy, A. Roussarie, J.-P. Schuller, J. Schwindling, A. Trabelsi, B. Vallage

CEA, DAPNIA/Service de Physique des Particules, CE-Saclay, 91191 Gif-sur-Yvette Cedex, France[17]

S.N. Black, J.H. Dann, R.P. Johnson, H.Y. Kim, N. Konstantinidis, A.M. Litke, M.A. McNeil, G. Taylor

Institute for Particle Physics, University of California at Santa Cruz, Santa Cruz, CA 95064, USA[22]

C.N. Booth, C.A.J. Brew, S. Cartwright, F. Combley, M.S. Kelly, M. Lehto, J. Reeve, L.F. Thompson

Department of Physics, University of Sheffield, Sheffield S3 7RH, United Kingdom[10]

K. Affholderbach, A. Böhrer, S. Brandt, G. Cowan, C. Grupen, P. Saraiva, L. Smolik, F. Stephan

Fachbereich Physik, Universität Siegen, 57068 Siegen, Fed. Rep. of Germany[16]

M. Apollonio, L. Bosisio, R. Della Marina, G. Giannini, B. Gobbo, G. Musolino

Dipartimento di Fisica, Università di Trieste e INFN Sezione di Trieste, 34127 Trieste, Italy

J. Rothberg, S. Wasserbaech

Experimental Elementary Particle Physics, University of Washington, WA 98195 Seattle, U.S.A.

S.R. Armstrong, E. Charles, P. Elmer, D.P.S. Ferguson, Y. Gao, S. González, T.C. Greening, O.J. Hayes, H. Hu, S. Jin, P.A. McNamara III, J.M. Nachtman,[24] J. Nielsen, W. Orejudos, Y.B. Pan, Y. Saadi, I.J. Scott, J. Walsh, Sau Lan Wu, X. Wu, J.M. Yamartino, G. Zobernig

Department of Physics, University of Wisconsin, Madison, WI 53706, USA[11]

1 Introduction

Semileptonic τ decays offer a rather clean environment for investigating the hadronic weak current. In recent years, a special interest in the experimental study of τ lepton decays into final states containing one or more kaons has developed. In view of the precision reached in the study of τ hadronic decays [1, 2], these modes should be measured in order to provide completely exclusive decay rates. Moreover, the decays with a $K\overline{K}$ pair appear to play a significant role for understanding the vector and axial-vector component in low-energy QCD studies [3], and those with only one kaon give access to the study of the strange sector of τ decays [3]. Since the dynamics of these decay channels is complicated by the presence of several hadrons in the final states with different possible resonance production, several models have been proposed, either based on $SU(3)$ symmetry breaking [4], or on chiral Lagrangians [5, 6, 7, 8].

In ALEPH, there are three ways to distinguish kaons from pions in τ decays. Charged kaons are identified by the dE/dx measurement and neutral kaons are identified according to their two components: K_S^0 and K_L^0. The K_S^0 decay into $\pi^+\pi^-$ is reconstructed by means of a vertex finding algorithm, and the K_L^0's are isolated by analyzing an excess of hadronic energy as measured in the calorimeters.

In this paper, K_S^0 production in τ decays is studied to measure branching ratios for the inclusive mode and the exclusive modes with one or two kaons. The analysis is arranged as follows. First, τ decays containing K_S^0's are selected. This allows the measurement of the inclusive branching ratio for $\tau^- \to K_S^0 X^- \nu_\tau$ where X^- can be anything (charge conjugate states are implied throughout this paper). Then, candidates are classified according to the number of K_S^0's, together with the number of accompanying π^0's and charged hadrons. K_L^0 components merged in the final states classified as $K_S^0 h^- \nu_\tau$ and $K_S^0 h^- \pi^0 \nu_\tau$ are extracted from fits to the hadronic energy excess distributions. Similarly, the ratios for charged kaon components in the $K_S^0 h^- \nu_\tau$ and $K_S^0 h^- \pi^0 \nu_\tau$ channels are obtained from the analyses of the accompanying primary charged hadron (h^-), using the dE/dx information as described in Ref. [9]. The study for the exclusive decays is performed in the order dictated by the respective background subtraction, giving the branching ratios for $\tau^- \to K_S^0 K_S^0 \pi^- (\pi^0)\nu_\tau$, $\tau^- \to K_S^0 K_L^0 \pi^- (\pi^0)\nu_\tau$, $\tau^- \to K_S^0 h^+ h^- h^- \nu_\tau$, $\tau^- \to K_S^0 K^- \pi^0 \pi^0 \nu_\tau$, $\tau^- \to K_S^0 \pi^- \pi^0 \pi^0 \nu_\tau$, $\tau^- \to K^0 K^- (\pi^0)\nu_\tau$ and $\tau^- \to \overline{K}^0 \pi^- (\pi^0)\nu_\tau$. Finally, mass spectra in the $K_S^0 K^-$, $K_S^0 K_L^0 \pi^-$, $K_S^0 \pi^-$ and $K_S^0 \pi^- \pi^0$ final states are investigated to understand the relevant decay dynamics.

The τ decays with three kaons, like $\tau^- \to \overline{K}^0 K^0 K^- \nu_\tau$, will not be taken into account because of the strong suppression by both the Cabibbo angle and the available phase space, which has already been confirmed by investigating the isospin symmetry related state $\tau^- \to K^- K^+ K^- \nu_\tau$ in Ref. [9]. Consequently, the remaining particles in the channels with two kaons are treated as pions in this analysis.

2 Detector and Data Sample

A detailed description of the ALEPH detector can be found elsewhere [10]. The features relevant for the present analysis are briefly mentioned in the following.

Charged particle momenta are measured by a magnetic spectrometer operating in an axial magnetic field of 1.5 T and consisting of three different detectors: a precision silicon vertex detector (VDET), a cylindrical inner drift chamber (ITC) with eight drift layers, and a large time projection chamber (TPC) that provides up to 21 space points. The transverse momentum resolution is $\sigma_{p_T}/p_T = 6 \times 10^{-4} p_T \oplus 0.005$ (p_T in GeV/c). The TPC provides also up to 338 samples of ionization loss that are used for particle identification.

The energy of photons and electrons is measured in the electromagnetic calorimeter (ECAL), a lead/wire-chamber sampling device of thickness 22 radiation lengths. The resolution is $\sigma_E/E = 0.18/\sqrt{E(\text{GeV})} \oplus 0.009$. It is read out by cathode pads organized in projective towers subtending a solid angle of $0.9° \times 0.9°$; the fine granularity of this detector is particularly suited for π^0 reconstruction.

The 1.2 m thick iron return yoke is interleaved with 23 layers of streamer tubes and acts as a hadron calorimeter (HCAL) giving an energy resolution of about $0.85/\sqrt{E(\text{GeV})}$. Finally, two double layers of streamer tubes outside the HCAL act as a muon detector.

The present analysis uses data collected by the ALEPH detector during the 1991-1995 running periods at LEP; this corresponds to about 200,300 produced τ pairs at a centre of mass energy around the Z peak.

One million Monte Carlo τ pairs, generated with KORALZ [11], are used to evaluate the relevant selection efficiencies and study the backgrounds from other τ decay channels. The background from non-τ events is estimated by means of 5.8 million Monte Carlo Z $\rightarrow$ $q\bar{q}$ events, generated with JETSET 7.4 [12]. Background from the two-photon process is totally negligible in this analysis.

3 Event selection and reconstruction

3.1 General selection criteria

The general $\tau^+\tau^-$ selection criteria described in Ref. [1] have been applied to the data sets with VDET information, selecting a sample of 159,281 events in the five data acquisition periods with an estimated background from non-τ events of $(0.85 \pm 0.10)\%$.

A primary charged hadron is defined as having at least four TPC coordinates, a momentum exceeding 300 MeV/c, an impact parameter less than 2 cm in the plane perpendicular to the beam axis and 10 cm in the direction parallel to it, and being not identified as an electron [13]. In this analysis, since the K_S^0 may decay far from the interaction point, the requirements on the impact parameter for the possible daughter charged hadrons (defined as the secondary charged hadrons) are relaxed to a distance of closest approach to the beam axis smaller than 100 cm. Because nuclear interactions in the ITC and TPC walls can produce many charged tracks, the number of secondary charged hadrons should not be more than four in the inclusive sample. In the exclusive modes, the candidate events should not contain any secondary charged hadron except for those used for the K_S^0 reconstruction.

Following Ref. [1], π^0's are defined as: (i) "resolved π^0" with a pair of photons constrained with the π^0 mass; and (ii) "unresolved π^0" with a high energy π^0 leading to a single cluster in the ECAL, where the two photons are reconstructed through a

2

cluster moment analysis. Events containing residual photons as defined in Ref. [1] are not used in the study of exclusive modes because of more background involved, as in particular from fake photons generated by hadronic interactions (including from K_L^0's) in ECAL.

3.2 $K_S^0 \to \pi^+\pi^-$ reconstruction

The decay $K_S^0 \to \pi^+\pi^-$ is reconstructed by pairing two oppositely charged hadrons in the same hemisphere defined by the thrust axis. Accidental pairings with primary tracks are strongly reduced by requiring no VDET hits on the pair of tracks, thus imposing a minimum K_S^0 decay length of 11 cm in the plane transverse to the beam.

A three-dimensional vertex fit without kinematic constraint is performed to reject background and improve the K_S^0 momentum resolution. A good K_S^0 candidate must satisfy the following conditions: (i) $\chi^2/ndf \leq 25$; (ii) the corresponding decay length L_{xy} in the plane perpendicular to the beam axis is required to be longer than 11 cm but shorter than 150 cm, where the lower limit corresponds to the external radius of the VDET, while the upper one is chosen to allow the tracks to have a minimum of four TPC coordinates; (iii) the impact parameter d_0^K of the K_S^0 candidate in x-y plane must be smaller than 2 cm; (iv) $\cos\alpha$, where α is the angle between the K_S^0 momentum and the direction from the intersection point to the K_S^0 decay vertex, must be greater than 0.995, in order to ensure further the pointing of the K_S^0 to the interaction point. This last cut also discards the wrong solution from the vertex finding algorithm. In case two good vertices are found with one common track, the solution with the longer L_{xy} is retained.

The distributions of χ^2/ndf, L_{xy} and d_0^K are shown in Fig. 1 for data and Monte Carlo. The distribution of $\cos\alpha$ in data is given in Fig. 2. A good K_S^0 signal always corresponds to $\cos\alpha$ very near 1.

Events with two K_S^0's are selected by tagging one K_S^0 with the requirements described above and the other K_S^0 with looser cuts: the VDET veto is not applied and the range of allowed L_{xy} is extended down to 2 cm.

Finally, all events are classified into the inclusive K_S^0 sample irrespectively of the accompanying primary particles, and into the exclusive K_S^0 samples according to the number of K_S^0's, the number of charged hadrons and the number of π^0's as follows: $K_S^0 K_S^0 h^-$, $K_S^0 K_S^0 h^- \pi^0$, $K_S^0 h^+ h^- h^-$, $K_S^0 h^- \pi^0 \pi^0$, $K_S^0 h^-$ and $K_S^0 h^- \pi^0$. To be consistent with a τ decay, the total hadronic invariant mass in all the exclusive modes is required to be smaller than 1.8 GeV/c^2, where the pion mass is assigned to the accompanying primary charged hadron. Contamination from the K_S^0 production due to the nuclear interactions in the ITC and TPC walls is estimated to be at a level of 10^{-3} in the exclusive modes and is therefore ignored in the following analysis, while the influence on the inclusive mode will be discussed in the section relevant to the systematic uncertainty.

4   Determination of the inclusive branching ratio

The invariant mass for the selected K_S^0 signal is shown in Fig. 3. The mass resolution is found to depend strongly on the momentum; in fact, at higher momenta, the tracks tend
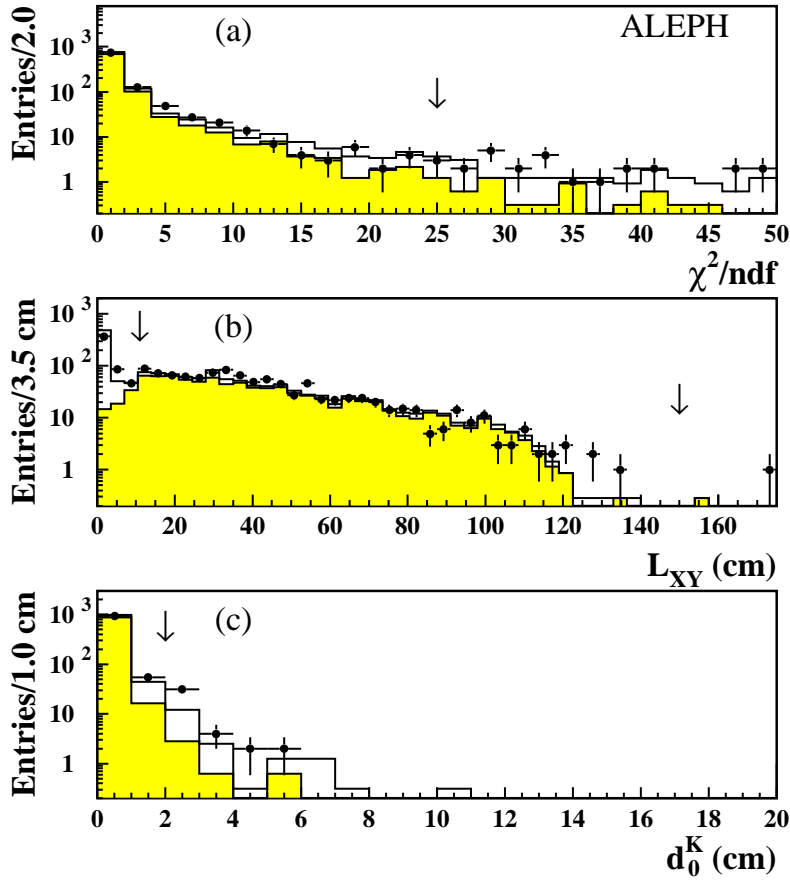
Figure 1: *Distributions of (a) χ^2/ndf, (b) decay length L_{xy} and (c) impact parameter d_0^K for neutral vertices, in which the K_S^0 mass windows described in Section 5, a 3 GeV/c minimum K_S^0 momentum and all other vertex cuts have already been applied, except for the quantity under study. The black points, open and shaded histograms are data, Monte Carlo predictions for all the neutral vertices, and the true K_S^0 signal. The last two plots are normalized to the same luminosity as in data. The corresponding cuts are indicated by the vertical arrows.*
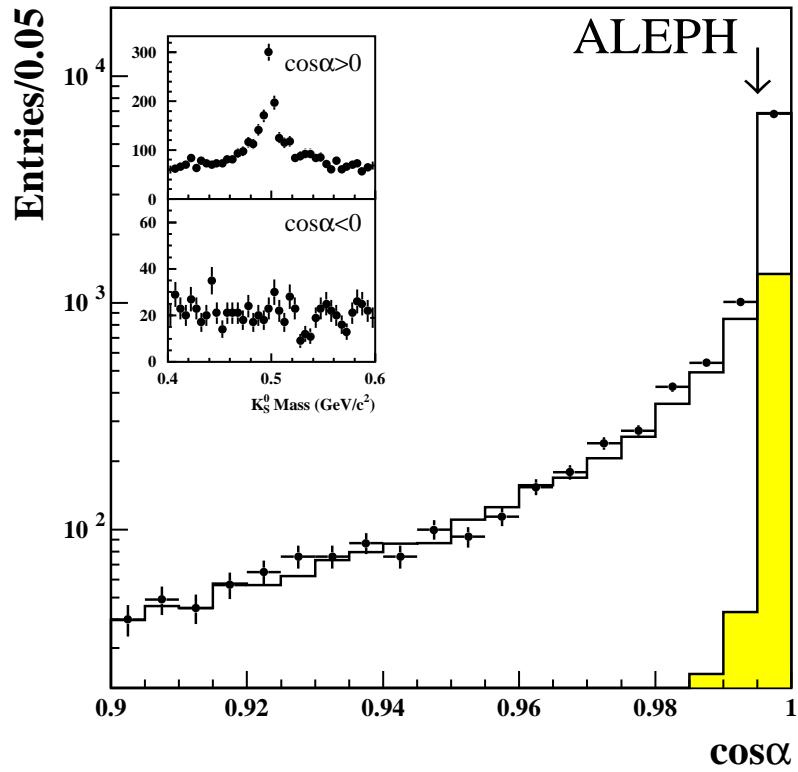
Figure 2: $\cos\alpha$ *distribution for data (black points). Monte Carlo predictions for all the neutral vertices and the true K_S^0 signal are shown in the open and shaded histograms, which are normalized to the same luminosity as in data. The cut is indicated by the vertical arrow. The inset plots correspond to the neutral vertices with the correct (positive $\cos\alpha$) and wrong (negative $\cos\alpha$) solutions in the K_S^0 finding algorithm.*

$p_{K_S^0}$ (GeV/c)	$N(K_S^0)$	$q\bar{q}$ background	ϵ (%)	$B_i(K_S^0 X^-)$ (10^{-3})
$0-5$	68.3 ± 15.3	27.5 ± 5.7	26.39 ± 3.15	0.39 ± 0.15
$5-10$	203.1 ± 19.5	16.7 ± 5.7	30.53 ± 0.75	1.52 ± 0.17
$10-15$	312.2 ± 21.6	9.1 ± 3.6	24.87 ± 0.51	3.04 ± 0.22
$15-20$	160.9 ± 19.4	7.0 ± 3.4	20.46 ± 0.53	1.88 ± 0.24
$20-25$	94.8 ± 20.5	2.0 ± 1.0	18.18 ± 0.76	1.27 ± 0.28
$25-30$	43.7 ± 9.6	4.0 ± 2.0	15.62 ± 0.91	0.63 ± 0.16
≥ 30	45.8 ± 11.0	6.9 ± 2.5	10.00 ± 0.78	0.97 ± 0.28

Table 1: K_S^0 momentum range, number of K_S^0's from the fits, estimated background from $q\bar{q}$, selection efficiency and partial branching ratio in each momentum slice. Errors are statistical only.

to be more overlapped and their lengths are, on average, shorter. To avoid any possible bias due to imperfect detector simulation and to increase the efficiencies, especially for the channels involving high momentum K_S^0's, the number of K_S^0's is estimated by fitting the mass spectrum in different momentum slices. The signal is represented by two Gaussians and the accidental background is described by a linear term.

The fit results for the inclusive mode are listed in Table 1, and the sum of fits to the K_S^0 mass spectrum in each momentum slice is shown in Fig. 3. Since the τ decaying into inclusive K_S^0's involves a priori unknown dynamics, the analysis performed with the sample split into momentum slices can reduce the systematic uncertainty on the efficiency, giving the opportunity for comparing the K_S^0 mass resolution between data and Monte Carlo. Some discrepancy is observed and a corresponding correction is applied to the simulated K_S^0 mass resolution as a function of momentum, and used in the estimates of relevant efficiencies. The branching ratio for the inclusive mode is computed via

$$B(\tau^- \to K_S^0 X^- \nu_\tau) = \frac{1}{2N_{\tau\tau}} \sum_i \frac{N_i(K_S^0) - N_i(q\bar{q})}{\epsilon_i}, \qquad (1)$$

where $N_i(K_S^0)$, $N_i(q\bar{q})$, ϵ_i are the number of K_S^0's from the fits, the estimated background of K_S^0's from $q\bar{q}$ and the signal efficiency for the i-th momentum bin as taken from Table 1. The $q\bar{q}$ background in each momentum slice is estimated from Monte Carlo within the mass region $(0.3 \sim 0.7)$ GeV/c^2. The result is obtained by adding the ratios in all the momentum slices, yielding

$$B(\tau^- \to K_S^0 X^- \nu_\tau) = (9.70 \pm 0.58_{stat.}) \times 10^{-3}. \qquad (2)$$

The momentum distribution of K_S^0 candidates in τ decays is shown in Fig. 4, together with the Monte Carlo prediction. The relative contributions of various exclusive decay channels are fixed in the simulation to the values of the exclusive branching ratios obtained in this analysis. The simulation agrees with the data.

6
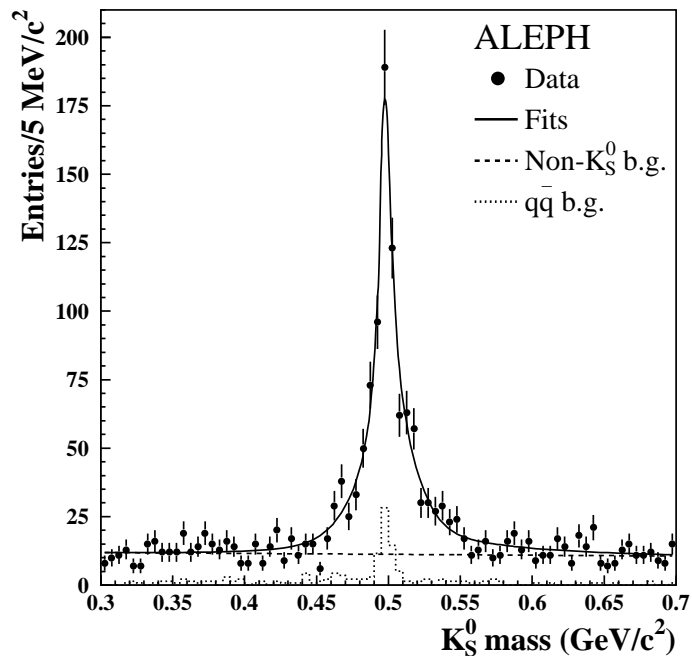
Figure 3: *Invariant mass distribution of the selected K_S^0 candidates (points with error bars). The solid curve is the sum of all the invariant mass fits corresponding to the individual K_S^0 momentum slices. The dashed curve indicates the fitted non-K_S^0 background, while the dotted histogram is for the expected $q\bar{q}$ background.*

Figure 4: *Momentum distribution of the K_S^0 candidates (points with error bars) in τ decay. Monte Carlo prediction is given by the histogram. The K_S^0 selection efficiency as a function of momentum is also shown below with triangles.*

7

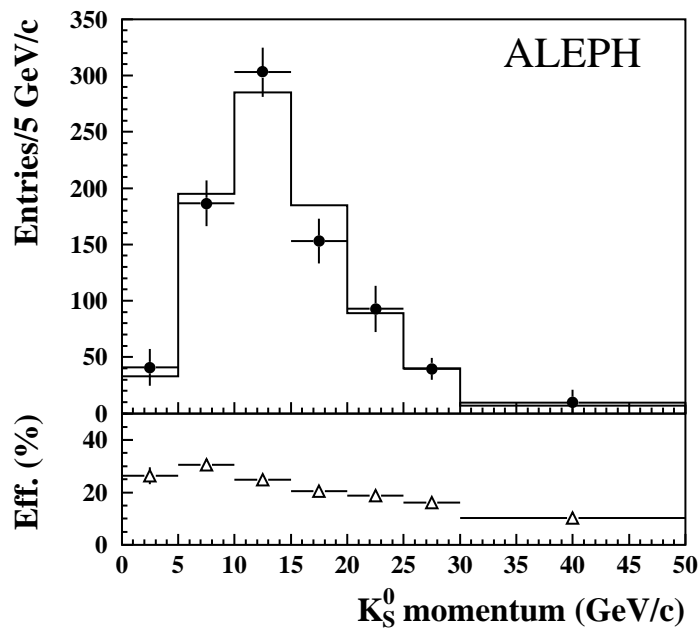|	$K_S^0 h^- \nu_\tau$			$K_S^0 h^- \pi^0 \nu_\tau$		
Mode	ϵ (%)	$\epsilon_{dE/dx}$ (%)	$\epsilon_{K_L^0}$ (%)	ϵ (%)	$\epsilon_{dE/dx}$ (%)	$\epsilon_{K_L^0}$ (%)
$K_S^0 \pi^-$	19.93 ± 0.42	–	–	0.20 ± 0.04	–	–
$K_S^0 K^-$	21.69 ± 0.84	13.30 ± 0.58	–	0.46 ± 0.14	0.33 ± 0.10	–
$K_S^0 \pi^- \pi^0$	1.89 ± 0.24	–	–	13.36 ± 0.59	–	–
$K_S^0 K^- \pi^0$	2.63 ± 0.35	1.26 ± 0.34	–	8.89 ± 0.46	4.62 ± 0.25	–
$K_S^0 K_L^0 \pi^-$	16.10 ± 0.57	–	14.30 ± 0.46	2.90 ± 0.18	–	2.58 ± 0.16
$K_S^0 K_S^0 \pi^-$	6.10 ± 0.49	–	–	3.45 ± 0.34	–	–
$K_S^0 K_L^0 \pi^- \pi^0$	2.52 ± 0.33	–	2.39 ± 0.31	8.98 ± 0.63	–	8.78 ± 0.61
$K_S^0 K_S^0 \pi^- \pi^0$	0.60 ± 0.24	–	–	3.50 ± 0.59	–	–
$K_S^0 \pi^- \pi^0 \pi^0$	0.24 ± 0.10	–	–	2.48 ± 0.32	–	–
$K_S^0 K^- \pi^0 \pi^0$	0.55 ± 0.09	0.30 ± 0.07	–	3.36 ± 0.22	1.92 ± 0.16	–

Table 2: *Efficiencies for the studied τ channels classified in the $K_S^0 h^- (\pi^0) \nu_\tau$ topologies. The global efficiency ϵ does not involve any K_S^0 mass window cut, while those efficiencies for $\epsilon_{dE/dx}$ and $\epsilon_{K_L^0}$ include the K_S^0 mass windows. Errors are statistical only. See text for details.*

5   The efficiency matrix for exclusive modes

The τ Monte Carlo samples are generated by the standard KORALZ generator [11], where the form factors for two-meson and three-meson τ decays are derived from Ref. [6, 7]. Since any discrepancy in the resonance structure between the model prediction and the data may cause a systematic bias, the efficiency matrix is corrected according to the total hadronic mass spectra as described in Sections 9 and 10. For the four-meson τ decays, a phase space generator [2] is used. Table 2 gives the relevant efficiencies for the topological $K_S^0 h^- (\pi^0) \nu_\tau$ samples. The global efficiency ϵ is defined for tagging a true K_S^0 without involving any cut on the K_S^0 mass. For the purpose of studying the $K_S^0 K_L^0 \pi^- (\pi^0)$ and $K_S^0 K^- (\pi^0)$ modes, individual $K_S^0 h^-$ and $K_S^0 h^- \pi^0$ candidates are further selected by means of K_S^0 mass windows (see Table 3), which tend to both remove non-K_S^0 background and avoid secondary systematic uncertainty due to the imperfect simulation of the K_S^0 mass resolution. Consequently, two specific efficiencies, $\epsilon_{dE/dx}$ and $\epsilon_{K_L^0}$ are introduced for the channels with one charged kaon and with one K_L^0. In order to compute the efficiency $\epsilon_{dE/dx}$, the definition of Ref. [9] for the charged kaon track with a reliable dE/dx measurement is used. The efficiency $\epsilon_{K_L^0}$ is only affected by the K_S^0 mass cuts. The efficiencies for the $K^0 h^+ h^- h^-$ and the $K^0 h^- \pi^0 \pi^0$ final states will be given in the relevant section.

6   Calorimetric determination of K_L^0 production

6.1   Hadronic energy calibration

In the $K_S^0 h^-$ and $K_S^0 h^- \pi^0$ samples, channels involving K_L^0 are found to have a sizeable contribution because of the unreconstructed K_L^0. Following Ref. [1], a variable measuring

---

[2]as used in TAUOLA [11] for the 4π channel with the V-A matrix element.

$p_{K_S^0}$ (GeV/c)	$0-5$	$5-10$	$10-15$	$15-20$	$20-25$	≥ 25
$m_{K_S^0}$ (GeV/c^2)	$0.48-0.52$	$0.47-0.53$	$0.45-0.55$	$0.42-0.58$	$0.4-0.6$	$0.4-0.75$

Table 3: K_S^0 mass windows used for the different K_S^0 momentum in the study of $K_S^0 K^-(\pi^0)$ and $K_S^0 K_L^0 \pi^-(\pi^0)$.

the hadronic energy excess from a K_L^0 contribution is defined as

$$\delta_E = \frac{E_{CAL} - (E_{\pi^0}) - \Sigma_i P_{Ch}^i}{\sigma}, \tag{3}$$

where E_{CAL} is the energy deposited in all calorimeters within a $30°$ cone along the thrust axis, E_{π^0} is the π^0 energy in the $K_S^0 h^- \pi^0$ mode, $\Sigma_i P_{Ch}^i$ is the sum of all charged hadron momenta and σ is taken as the square root of the sum of the charged hadron momenta in GeV/c. With this definition, the mean of δ_E for the decay $\tau^- \to K_S^0 h^-(\pi^0)\nu_\tau$ is expected to be zero. The presence of the K_L^0 component in the decay $\tau^- \to K_S^0 K_L^0 h^-(\pi^0)\nu_\tau$ shifts the mean of δ_E to around 2, which makes it possible to statistically isolate the K_L^0 signal.

Samples of $\tau^- \to h^+ h^- h^- \nu_\tau$ and $\tau^- \to h^+ h^- h^- \pi^0 \nu_\tau$ decays are used to calibrate the δ_E according to (i) the period of data acquisition; (ii) the polar angle of the jet; (iii) the sum of the momenta of the charged tracks. To minimize the K_L^0 contamination in the $h^+ h^- h^-$ mode, the invariant mass of the $3h$ system (computed with the assumption that the three hadrons are pions) is required to be greater than 1.1 GeV/c^2. Corrections to the mean value of δ_E and its resolution are applied to the Monte Carlo samples to match the data. These corrections are then applied to the $K_S^0 h^-$ and $K_S^0 h^- \pi^0$ modes separately.

6.2 Fitting the K_L^0 fractions

For the $K_S^0 K_L^0 \pi^-(\pi^0)\nu_\tau$ channels, the kinematics require the invariant mass of the $K_S^0 \pi^-(\pi^0)$ system to be less than $(m_\tau - m_{K_L^0})$. In practice, the mass is required to be less than 1.3 GeV/c^2. This cut enhances the K_L^0 component in the $K_S^0 h^-(\pi^0)$ samples. The numbers of surviving candidates are 467 and 77 for the $K_S^0 h^-$ and the $K_S^0 h^- \pi^0$ samples, respectively.

The shapes of the δ_E distributions for the $K_S^0 h^-(\pi^0)$ modes are first taken from Monte Carlo τ decays, including the backgrounds. The effects of imperfect detector simulation are then corrected as stated above. A binned maximum likelihood fit is then performed to extract the K_L^0 fractions (see Table 4). It is noted that the $K^0 \overline{K}^0 \pi^- \nu_\tau$ channel can feed into the $K_S^0 h^- \pi^0$ sample, when one of the K^0's mainly interacts in the ECAL, resulting in a fake π^0 reconstructed due to part of the K^0 shower. Since the energy of this "π^0" is subtracted from the hadronic energy, the remaining energy, according to the simulation, gives a smaller mean of δ_E (~ 0.85) in the analysis of $K_S^0 K_L^0 \pi^- \pi^0$. This small effect is taken into account in the fit to the $K_S^0 h^- \pi^0$ sample. Fig. 5 illustrates the K_L^0 contributions in both modes.

Sample	$f_{K_L^0}$ (%)	$N_{K_L^0}$	χ^2/ndf
$K_S^0 h^-$	14.6 ± 2.7	68 ± 13	$25.1/31$
$K_S^0 h^- \pi^0$	13.9 ± 5.8	11 ± 4	$10.5/18$

Table 4: *Results from the fits to δ_E distributions. The fraction of K_L^0 ($f_{K_L^0}$) and the corresponding number of K_L^0's ($N_{K_L^0}$) are given with statistical uncertainties only. The χ^2 gives an indication of the quality of the likelihood fits.*

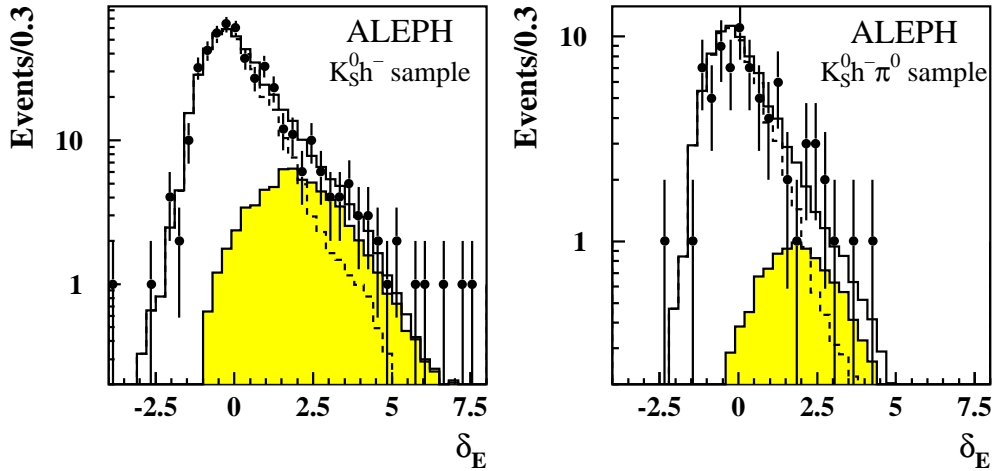Figure 5: *Hadronic energy excess distributions for (a) the $K_S^0 h^-$ and (b) the $K_S^0 h^- \pi^0$ samples, where the K_S^0's are selected with the mass windows. Data are shown as points with error bars, while Monte Carlo predictions are given by open histograms. The shapes for the $K_S^0 h^- (\pi^0)$ samples and the $K^0 \overline{K}^0 \pi (\pi^0)$ signals are shown in dashed and shaded separately.*

Mode	M.C. $\bar{x}_\pi(K)$	M.C. $\sigma_\pi(K)$	f_K (%)	N_K	χ^2/ndf
$K_S^0 h^-$	-1.92 ± 0.05	1.09 ± 0.03	11.9 ± 2.7	46 ± 11	$18.8/34$
$K_S^0 h^- \pi^0$	-1.69 ± 0.11	1.15 ± 0.08	12.6 ± 6.0	15 ± 7	$9.1/12$

Table 5: *Results from the fits to the x_π distributions for the primary charged hadrons in the $K_S^0 h^-$ and $K_S^0 h^- \pi^0$ final states. The fraction of charged kaon content f_K and the number of charged kaons N_K are given with statistical uncertainties only. The χ^2 gives an indication of the quality of the likelihood fits.*

7   Identification of charged kaons by dE/dx

In this analysis, dE/dx measurement is applied to separate $K_S^0 K^- (\pi^0)$ from $K_S^0 \pi^- (\pi^0)$. The dE/dx calibration used in Ref. [9] can be applied, since most of the $K_S^0 h^- (\pi^0)$ modes (90%) with $K_S^0 \to \pi^+ \pi^-$ are in the selected $3h^-$ and $3h^- \pi^0$ final states. The same technique of statistical particle identification is used to extract the charged kaon content and measure the branching ratios for the decays $K_S^0 K^- \nu_\tau$ and $K_S^0 K^- \pi^0 \nu_\tau$. For each charged track accompanying a K_S^0, the measured ionization loss R is compared to the expected value R_π for pions using the estimator

$$x_\pi = \frac{R - R_\pi}{\sigma_\pi}, \tag{4}$$

where σ_π is the expected resolution for pions. The pion dE/dx response and the $x_\pi(\pi)$ parameters (namely, $\bar{x}_\pi$ and σ_π) are the same as used in Ref. [9]. By means of Monte Carlo simulation, the $x_\pi(K)$ parameters are determined specifically for the $K_S^0 K^-$ and $K_S^0 K^- \pi^0$ modes. To enhance the kaon fraction, a cut at 1.8 GeV/c^2 is imposed on the invariant mass $K_S^0 h^- (\pi^0)$, assuming a kaon mass for the primary charged hadron. The fit results are given in Table 5. Fig. 6 shows the x_π distributions for both $K_S^0 h^-$ and $K_S^0 h^- \pi^0$ candidates. A kaon signal can be seen in the low x_π tail of the distribution.

8   Determination of the exclusive branching ratios

All exclusive branching ratios involving one or two K_S^0's are determined in this section. Since the measurements on these channels are correlated as shown in Table 2, the simplest way of proceeding is to start with the channels involving the least background.

8.1   Channels involving two K_S^0's

A study of $\tau^- \to K_S^0 K_S^0 \pi^- (\pi^0) \nu_\tau$ is performed first. The relaxed selection criteria described in Section 3 are applied. For the $K_S^0 K_S^0 \pi^-$ mode, 6 candidates with a negligible background (< 0.2) are found within the ± 100 MeV/c^2 K_S^0 mass box (see Fig. 7). The number of events outside the K_S^0 mass box is 3, in agreement with the 2.2 expected from the simulation of the background. No candidate is observed in the $K_S^0 K_S^0 \pi^- \pi^0$ sample.
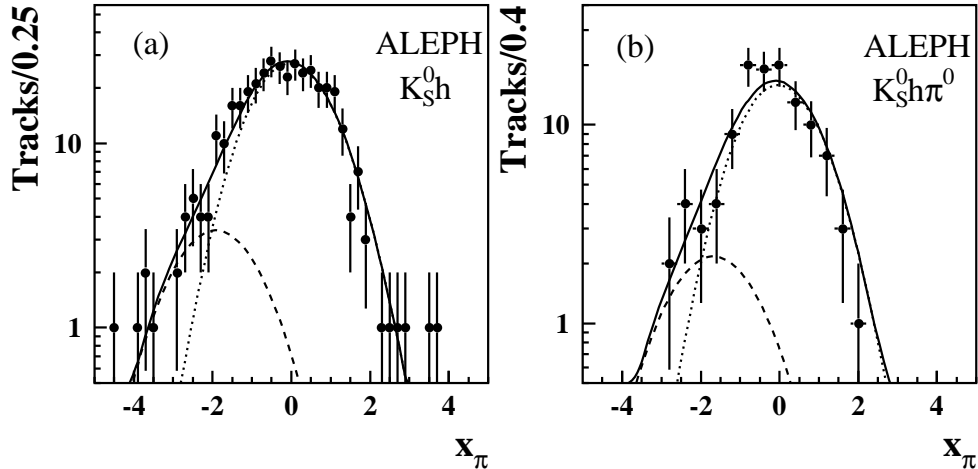
Figure 6: *Fitted x_π distributions for the isolated charged tracks in (a) the $K_S^0 h^-$ sample and (b) the $K_S^0 h^- \pi^0$ sample, where the K_S^0's are selected by the mass windows. The points with error bars correspond to data, the dashed curves show the fitted K component distributions, and the dotted curves show the expected π component distributions.*

The efficiencies are estimated to be $(5.86 \pm 0.38)\%$ and $(3.6 \pm 0.30\%)$ for the $K_S^0 K_S^0 \pi^-$ and the $K_S^0 K_S^0 \pi^- \pi^0$ modes. The branching ratios are

$$B(\tau^- \to K_S^0 K_S^0 \pi^- \nu_\tau) = (0.26 \pm 0.10_{stat.}) \times 10^{-3}, \tag{5}$$

and

$$B(\tau^- \to K_S^0 K_S^0 \pi^- \pi^0 \nu_\tau) < 0.20 \times 10^{-3} \ (95\% \ C.L.). \tag{6}$$

8.2 Channels involving a $K_S^0 K_L^0$ pair

The channels $K_S^0 K_L^0 \pi^- \nu_\tau$ and $K_S^0 K_L^0 \pi^- \pi^0 \nu_\tau$ are investigated. The background from the decay $K_S^0 K_L^0 K^- (\pi^0) \nu_\tau$ can be neglected, while the $q\bar{q}$ background contributes 1.4 ± 1.0 events to the $K_S^0 h^-$ sample with large δ_E. The K_L^0 contributions are obtained from fits to the δ_E distribution (see Table 4), yielding the branching ratios

$$B(\tau^- \to K_S^0 K_L^0 \pi^- \nu_\tau) = (1.01 \pm 0.23_{stat.}) \times 10^{-3}, \tag{7}$$

and

$$B(\tau^- \to K_S^0 K_L^0 \pi^- \pi^0 \nu_\tau) = (0.31 \pm 0.11_{stat.}) \times 10^{-3}. \tag{8}$$

In the computation of the branching ratio $B(\tau^- \to K_S^0 K_L^0 \pi^- \nu_\tau)$, a correction of $(-0.10 \pm 0.04) \times 10^{-3}$ is applied to account for those $K_S^0 K_S^0 \pi^- \nu_\tau$ events in which one of the K_S^0's does not decay inside the fiducial tracking volume but interacts in the HCAL, thus behaving like a K_L^0. Also, if the π^0 in $K_S^0 K_L^0 \pi^- \pi^0 \nu_\tau$ is lost in the reconstruction,
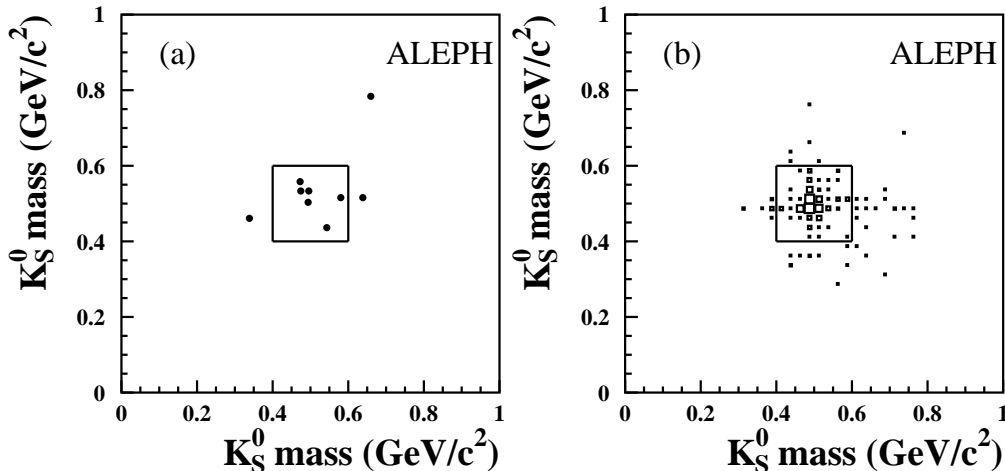
12

Figure 7: *Scatter plots for the invariant K_S^0 masses in the $K_S^0 K_S^0 \pi^-$ mode: (a) data, (b) Monte Carlo predictions for signal are shown. The box indicates the K_S^0 mass window for isolating the signal.*

this channel becomes a background in the decay $K_S^0 K_L^0 \pi^- \nu_\tau$ and gives almost the same distribution of δ_E as that for $K_S^0 K_L^0 \pi^- \nu_\tau$. A correction of $(-0.05 \pm 0.02) \times 10^{-3}$ for the branching ratio is therefore applied in obtaining $B(\tau^- \to K_S^0 K_L^0 \pi^- \nu_\tau)$.

8.3 Channels involving a K_S^0 and three accompanying mesons

A search for $K_S^0 h^+ h^- h^-$ and $K_S^0 h^- \pi^0 \pi^0$ hadronic states is also performed. In order to reduce the combinatorial background, the K_S^0 mass window is restricted to be $0.45 - 0.55$ GeV/c^2. The numbers of K_S^0 candidates are 6 and 12 for the two modes separately. The backgrounds are estimated to be 3.0 ± 0.3 (dominated by $K_S^0 K_S^0 \pi^-$) and 4.6 ± 1.0 events (with 1.4 ± 0.6 events from the combinatorial background, 1.4 ± 0.5 events from the $K_S^0 \pi^- \pi^0$ mode and 1.8 ± 0.6 events from the $K_S^0 K_S^0 \pi^-$ mode). Since events with high multiplicity may suffer contamination from the nuclear interactions in the detector material, a check on the L_{xy} is done. No peak is observed in the positions corresponding to the ITC and TPC walls, the background being strongly suppressed by the cuts on the K_S^0 mass and the total hadronic invariant mass. Three different decay channels contribute to the $K_S^0 h^+ h^- h^- \nu_\tau$ final state: $K_S^0 K^+ \pi^- \pi^- \nu_\tau$, $K_S^0 K^- \pi^+ \pi^- \nu_\tau$ and $K_S^0 \pi^- \pi^+ \pi^- \nu_\tau$. There is no way to separate them because of low statistics. Assuming that all three channels contribute equally, giving a mean efficiency of $(6.60 \pm 0.36)\%$, the $K_S^0 h^+ h^- h^-$ branching ratio is estimated

$$B(\tau^- \to K^0 h^+ h^- h^- \nu_\tau) = (0.23 \pm 0.19_{stat.}) \times 10^{-3}. \tag{9}$$

13

The dE/dx analysis of the charged track in the $K^0 h^- \pi^0 \pi^0$ sample is done after requiring an invariant mass cut $M(K^0_S K^- \pi^0 \pi^0) \leq 1.8$ GeV/c^2, reducing the number of candidates down to 6 events, in which 5 have a dE/dx measurement. A maximum likelihood fit to the x_π distribution, yields 0 ± 1.0 events for the $K^0_S K^- \pi^0 \pi^0$ mode. The efficiency $\epsilon_{dE/dx}$ is estimated to be $(2.10 \pm 0.20)\%$ for $K^0_S K^- \pi^0 \pi^0$, giving

$$B(\tau^- \to K^0 K^- \pi^0 \pi^0 \nu_\tau) < 0.39 \times 10^{-3} \ (95\% \ C.L.). \tag{10}$$

The efficiency for the decay mode $\tau^- \to K^0_S \pi^- \pi^0 \pi^0 \nu_\tau$ is $(6.36 \pm 0.48)\%$, yielding a branching ratio

$$B(\tau^- \to K^0 \pi^- \pi^0 \pi^0 \nu_\tau) = (0.58 \pm 0.33_{stat.}) \times 10^{-3}, \tag{11}$$

where the uncertainty from $K^0_S K^- \pi^0 \pi^0 \nu_\tau$ is included.

8.4 Channels involving a $K^0_S K^-$ pair

The combinatorial background from the $K^- \pi^+ \pi^- (\pi^0) \nu_\tau$ and $K^- K^+ \pi^- (\pi^0) \nu_\tau$ channels can be neglected in the $K^0_S h^-$ and $K^0_S h^- \pi^0$ modes. Also, the contamination from $q\bar{q}$ events becomes negligible when requiring a total invariant mass smaller than 1.8 GeV/c^2. Therefore, the $K^0_S K^- \nu_\tau$, $K^0_S K^- \pi^0 \nu_\tau$ and $K^0_S K^- \pi^0 \pi^0 \nu_\tau$ modes are the only ones contributing charged kaons in the $K^0_S h^-$ and the $K^0_S h^- \pi^0$ samples. The fits to the corresponding x_π distributions yield the charged kaon numbers listed in Table 5, providing the measurements

$$B(\tau^- \to K^0 K^- \nu_\tau) = (1.58 \pm 0.42_{stat.}) \times 10^{-3}, \tag{12}$$

and

$$B(\tau^- \to K^0 K^- \pi^0 \nu_\tau) = (1.52 \pm 0.76_{stat.}) \times 10^{-3}. \tag{13}$$

8.5 Channels involving a $K^0_S \pi^-$ pair

In each of the $K^0_S h^-$ and $K^0_S h^- \pi^0$ final states, the dominant branching ratios of the $K^0_S \pi^- (\pi^0) \nu_\tau$ channels can be extracted using the full statistics, not requiring the dE/dx information for the accompanying primary charged particle or imposing the K^0_S mass windows. As done for the inclusive mode, the numbers of $K^0_S h^- (\pi^0)$ are taken directly from the fits to the invariant mass of K^0_S candidates. Since K^0_S candidates in the $K^0_S h^-$ mode have a broad momentum spectrum, they are divided into two parts: one with K^0_S momenta below 15 GeV/c and the other one above 15 GeV/c, in order to simplify the parametrization of the resolution of the K^0_S signal. The corresponding K^0_S mass distributions are fitted to give a number of 509 ± 40 candidates in the $K^0_S h^-$ sample, in which Monte Carlo predicts 5 ± 2 of the $q\bar{q}$ background. For the $K^0_S h^- \pi^0$ mode, the number of K^0_S's is found to be 142 ± 13 from the global fit and the $q\bar{q}$ contamination is estimated to be 2 ± 1. Taking into account the measured $K^0_S K^- (\pi^0)$, $K^0_S K^0_L \pi^- (\pi^0)$, $K^0_S K^0_S \pi^-$ and $K^0_S \pi^- \pi^0 \pi^0$ branching ratios, the $q\bar{q}$ backgrounds, and the efficiencies listed in Table 2, the branching ratio for $K^0_S \pi^-$ can be obtained by the expression

$$B(\tau^- \to K^0_S \pi^- \nu_\tau) = \frac{N(K^0_S h^-) - N_{q\bar{q}}(K^0_S h^-)}{2 N_{\tau\tau} \epsilon(K^0_S \pi^-)} - \sum_i B(i) \frac{\epsilon(i)}{\epsilon(K^0_S \pi^-)}, \tag{14}$$

where N is the number of K_S^0 events from the fits, $B(i)$ is the i-th relevant τ branching ratio and $\epsilon(i)$ is the corresponding efficiency given in Table 2, without involving any dE/dx measurement or the K_S^0 mass windows. A similar expression is also used for deriving the branching ratio for $K_S^0 \pi^- \pi^0$. The results are

$$B(\tau^- \to \overline{K}^0 \pi^- \nu_\tau) = (8.55 \pm 1.17_{stat.}) \times 10^{-3}, \tag{15}$$

and

$$B(\tau^- \to \overline{K}^0 \pi^- \pi^0 \nu_\tau) = (2.94 \pm 0.73_{stat.}) \times 10^{-3}. \tag{16}$$

9   Systematic uncertainties

The main sources of systematic uncertainties listed in Table 6 come from the event selection, the K_S^0 selection criteria, the dE/dx measurement, the hadronic energy excess measurement, the evaluation of the background, the Monte Carlo statistics and the decay dynamics.

9.1   Selection efficiency

General τ-pair selection uncertainties are studied in Ref. [1]. In particular, for the $h^+ h^- h^- \nu_\tau$ and $h^+ h^- h^- \pi^0 \nu_\tau$ modes, the uncertainties due to the requirement of three charged hadrons and the handling of fake photons are addressed in Ref. [9]. However, the situation in $K_S^0 h^- \nu_\tau$ and $K_S^0 h^- \pi^0 \nu_\tau$ is slightly different because of the less stringent requirement for the tracks from K_S^0 decay. A factor 1.009 ± 0.009 is determined for the overestimation of the track reconstruction efficiency in simulated $K_S^0 h^- (\pi^0) \nu_\tau$ decays, while for the channels involving five charged tracks, the factor is found to be 1.03 ± 0.03.

The efficiency overestimation due to fake photons produced by hadron interactions in ECAL is the same as used in Ref [9] except for the decay involving two π^0's, where the correction is reduced since the loss of decays caused by the validation of an extra photon is partially compensated by the accidental reconstruction of a π^0 due to the presence of a fake photon. The corresponding factor is found to be 1.006 ± 0.018.

The efficiencies in Table 2 are already corrected by the above three factors.

9.2 K_S^0 selection criteria

About 20% of the K_S^0 vertices are lost inside the fiducial volume because one of the two tracks has less than four associated TPC coordinates. A study performed on a sample of three-prong events enriched in conversions, shows that track losses are correctly reproduced by the Monte Carlo to within 0.4%. A similar study performed on $\tau^- \to 3h^- \nu_\tau$ decays shows an agreement within 0.7%, which is assigned to the corresponding systematic uncertainty.

Interactions on the ITC and TPC walls can also produce hadrons, which affect the inclusive and the exclusive modes differently. In the inclusive mode, to avoid too many fake combinations between these hadrons, no more than four secondary good charged hadrons are permitted. In the simulation, at most four secondary good charged hadrons

are produced in good events, essentially in the $K^0_S K^0_S \pi^-$ mode; Monte Carlo shows that the possible loss due to this cut can be neglected. However, in the data, the fit to the K^0_S mass spectrum for hemispheres with more than four secondary charged hadrons shows a possible loss of K^0_S's amounting to a 0.7% of the total signal, which is taken as the systematic uncertainty for the inclusive channel, related to this cut.

In the study of the exclusive modes the presence of any secondary good charged hadron produced by the interactions results in the loss of decay candidates. In order to study the systematic uncertainty connected to this effect, test samples of $h^-(\pi^0)$ and $h^+ h^- h^-(\pi^0)$ events are selected according to the prescriptions of Ref. [1]; the cut on the number of secondary good charged hadrons is then removed and the variation in the number of selected events is studied in both data and Monte Carlo. The Monte Carlo predictions agree with data to within 1.5%, which is assigned as systematic error to the $K^0_S h(\pi^0)$ and the $K^0_S h \pi^0 \pi^0$ channels. For the final states involving five charged hadrons, a 1.0% uncertainty is estimated to the $K^0_S K^0_S \pi^-$ and the $K^0_S 3h^-$ modes.

Other sources of systematic effects are the secondary vertex finding algorithm which involves the VDET hit veto, the particle identification (PID) and the vertex fit. About 4% of the K^0_S's satisfying all other requirements are rejected because of a wrong association of a VDET hit to one of the two charged tracks. It is therefore important to study the correct reproduction of this effect in the simulation. For this purpose, the vertices with VDET hits and $L_{xy} > 11$ cm are investigated. The observed numbers of fitted K^0_S's between data and Monte Carlo are in agreement within 2.5%, which is thus quoted as the systematic uncertainty due to the VDET veto.

Particle identification is used to veto the electrons from photon conversions. It is found that pions erroneously identified as electrons account for about 3% inefficiency on the total signal; if no particle identification is required, a maximum relative variation of 2% is observed in the main branching ratios, and this is taken as the related systematic uncertainty.

Monte Carlo shows that 2% of the $K^0_S \to \pi^+ \pi^-$ are lost due to non-convergence of the vertex fit. Since there is no direct way to check this prediction in the data, this number is entirely taken as the systematic uncertainty for all the modes.

Systematic effects due to the χ^2, L_{xy}, d^K_0 and $\cos \alpha$ cuts are also investigated. Of prime interest is the study of the L_{xy} cut, which removes about 25% of the K^0_S's. For this purpose, decay candidates are selected both in data and Monte Carlo, without imposing the L_{xy} cut, but still keeping the VDET veto. Their L_{xy} distributions show a sharp rise corresponding to the VDET radial position, smeared by the effect of resolution. The effective VDET external radius and the L_{xy} resolution found in fits to these distributions in data and Monte Carlo are in a good agreement; the observed deviations are used to estimate systematic uncertainties on the efficiencies, yielding 2.0% and 0.6% for the effective radius and the resolution, respectively.

The other cuts remove less than 5% of remaining signal and thus do not introduce any significant systematic uncertainty. Conservatively, an uncertainty of 1% is assigned to each of them.

The estimates of the K^0_S mass window efficiencies depend on how well the corrected Monte Carlo reproduces the K^0_S mass resolution. This is studied by applying the mass windows used in the $K^0_S K^-(\pi^0)$, $K^0_S K^0_L \pi^-(\pi^0)$, and $K^0_S K^- \pi^0 \pi^0$ analyses to the inclusive

Source	τ sel	K_S^0 sel	dE/dx	δ_E	bkg	MC stat	Dynam	Total
$K_S^0 X^-$	1.5	4.8	–	–	3.5	1.4	1.2	6.4
$\overline{K}^0 \pi^-$	1.2	4.9	–	–	5.4	2.1	0.4	7.7
$\overline{K}^0 \pi^- \pi^0$	2.0	4.9	–	–	8.5	4.4	6.3	12.6
$K^0 K^-$	1.2	5.1	6.2	–	0.4	4.4	5.1	10.6
$K^0 K^- \pi^0$	2.0	5.1	9.7	–	0	5.4	5.3	13.5
$K_S^0 K_L^0 \pi^-$	1.2	5.1	–	9.2	0	3.2	5.6	12.4
$K_S^0 K_S^0 \pi^-$	13.5	5.7	–	–	3.3	6.5	6.0	17.4
$K_S^0 K_L^0 \pi^- \pi^0$	2.0	5.1	–	11.2	0	6.9	10	17.4
$\overline{K}^0 \pi^- \pi^0 \pi^0$	13.6	4.9		–	13.3	7.5	10	23.3
$K^0 h^+ h^- h^-$	13.5	5.7	–	–	21.6	5.5	18	32.2

Table 6: *Summary of systematic errors. A breakdown of the systematic uncertainties for K_S^0 selection is presented in Table 7. All are relative in percent.*

Mode	$K^0 X^- \nu_\tau$	$K^0 h^- \nu_\tau$	$K^0 h^- \pi^0 \nu_\tau$	$K_S^0 K_S^0 \pi^- \nu_\tau$	$K^0 h^+ h^- h^- \nu_\tau$	$K^0 h^- \pi^0 \pi^0 \nu_\tau$
Track loss	0.7	0.7	0.7	0.7	0.7	0.7
Interaction	0.7	1.5	1.5	1.0	1.0	1.5
PID	2.0	2.0	2.0	2.0	2.0	2.0
VDET	2.5	2.5	2.5	2.5	2.5	2.5
Vertex fit	2.0	2.0	2.0	2.0	2.0	2.0
χ^2	1	1	1	1	1	1
L_{xy}	2.1	2.1	2.1	2.1	2.1	2.1
d_0^K	1	1	1	1	1	1
$cos\alpha$	1	1	1	1	1	1
$M_{K_S^0}$	–	–	–	3.0	3.0	–
total	4.8	4.9	4.9	5.7	5.7	4.9

Table 7: *Contributions to the systematic error on K_S^0 selection (relative, in percent). See text for an explanation of the sources.*

sample; $(94.3 \pm 0.7)\%$ of the data and $(93.6 \pm 0.3)\%$ of the Monte Carlo events are kept by this cut. The two numbers agree within an accuracy of 1.5%, which is assigned to be the systematic error due to the K_S^0 mass cut. For the above mentioned channels this error is combined with the final one reported in Table 7 for the $K_S^0 h^-$, the $K_S^0 h^- \pi^0$ and the $K_S^0 h^- \pi^0 \pi^0$ modes to give the uncertainties listed in the second column of Table 6. For the $K_S^0 K_S^0 \pi^-$ and the $K^0 3h^-$ modes, different K_S^0 mass window cuts are applied. An uncertainty of 3.0% is assigned to both decay modes.

9.3   dE/dx measurement

The uncertainties associated with particle identification by dE/dx arise from pion dE/dx calibration, the dE/dx track efficiency, and the $x_\pi(K)$ parameters. Since the $K_S^0 h^-$ and $K_S^0 h^- \pi^0$ samples are very similar to the $h^+ h^- h^- (\pi^0)$ final states studied in Ref. [9], the same method is used to study the systematic uncertainties, yielding a 0.15% absolute

error on the charged kaon fraction due to the first two systematic uncertainties. This uncertainty is propagated into the channels involving a charged kaon and gives 1.3% for $\tau^- \to K_S^0 K^- \nu_\tau$ and 1.2% for $\tau^- \to K_S^0 K^- \pi^0 \nu_\tau$. The dE/dx track efficiency depends on the angle between the primary charged track and the other two tracks from K_S^0 decay. To simplify the procedure of estimating the systematic effect, an investigation of the invariant mass of the charged hadron system is performed as in Ref. [9]. The dE/dx sample efficiencies for data and Monte Carlo in the total three-prong sample agree and show a slight dependence on the invariant mass. Assuming the primary charged hadron to be a pion, the means of $M(\pi^+ \pi^- \pi^-)$ for $K_S^0 K^-$ and $K_S^0 K^- \pi^0$ are found to be about 1.2 GeV/c^2 and 0.9 GeV/c^2, respectively. The difference in the means between data and Monte Carlo invariant masses corresponds to systematic uncertainties on the efficiencies of 3.8% for $K_S^0 K^-$ and 5.4% for $K_S^0 K^- \pi^0$. For the $x_\pi(K)$ parameters, changing the values within one standard deviation listed in Table 5 gives the uncertainties due to the statistical errors of the $x_\pi(K)$ parameters: 4.7% for the $K_S^0 K^-$ mode and 7.9% for the $K_S^0 K^- \pi^0$ mode.

9.4   Hadronic energy excess

In the extraction of the branching ratios involving a K_L^0, the δ_E distribution for $K_S^0 h^- (\pi^0)$ events is used, taking into account the corrections derived from the observed difference between data and Monte Carlo in the $h^+ h^- h^- (\pi^0)$ mode as stated in Section 6.2. The effect of these corrections is a 7.1% variation of the K_L^0 fraction in the $K_S^0 K_L^0 \pi^- \nu_\tau$ sample, and 9.0% in the $K_S^0 K_L^0 \pi^- \pi^0 \nu_\tau$ one. A systematic uncertainty equal to these variations is thus associated to the two respective branching ratios. There is still another systematic source which can affect the δ_E distribution for $K_S^0 h$ events. In the $K_S^0 h$ sample, about 3.5% of the events are due to $K_S^0 h^- \pi^0$ decays in which the shower of the π^0 overlaps with one produced by a charged particle. This effect is taken into account in the fit to the $K_S^0 h^-$ sample. However, from the 15% uncertainty on the $K_S^0 h^- \pi^0$ branching ratio, a 5.8% uncertainty on the K_L^0 fraction for the $K_S^0 K_L^0 \pi^-$ mode is derived. Similarly, the dominant background channels for $K_S^0 K_L^0 \pi^- \pi^0$ are $K^0 \overline{K}^0 \pi^-$ (in which $K_S^0 \to \pi^0 \pi^0$) and $K^0 h^- \pi^0 \pi^0$, and the resulting uncertainty is estimated to be 6.7%

9.5   Background subtraction

Since the non-K_S^0 backgrounds in the $K_S^0 X^- \nu_\tau$ and $K_S^0 h^- (\pi^0) \nu_\tau$ modes are directly measured in the mass fit to data, the corresponding statistical errors are already taken into account. Also, the statistical uncertainty in the evaluation of the backgrounds are absorbed into an overall statistical error. Generally, the background in the channels involving a charged kaon is small and is ignored. The main effect of the background in the channels involving a K_L^0 is a change in the shape of the relevant δ_E distributions, which is taken into account in Section 9.4. Systematic uncertainties on branching ratios for all the background channels are propagated into $\overline{K}^0 \pi^- (\pi^0)$ because of the background subtraction, weighting the relevant efficiency matrix in Table 2. The systematic uncertainties are found to be 5.4% for $\overline{K}^0 \pi^-$ and 8.5% for $\overline{K}^0 \pi^- \pi^0$.

The uncertainty in the $q\bar{q}$ background affects only the inclusive mode significantly. A test on the $q\bar{q}$ background is performed by requiring $p_{K_S^0} \leq 5$ GeV/c and the K_S^0 hemisphere being with at least two accompanying hadrons. With these requirements, K_S^0 production from τ decays is reduced to a negligible level while most of the $q\bar{q}$ background is preserved. The predicted 21 ± 4 K_S^0's from the $q\bar{q}$ background is consistent with the obtained 22 ± 7 K_S^0's from the fit to data. This direct test involves only one third of the estimated $q\bar{q}$ contamination dominated by K_S^0 production in the low multiplicity fragmentation of $u\bar{u}$ and $d\bar{d}$ primary pairs. The remaining higher K_S^0 momentum contribution comes mostly from $s\bar{s}$ and should be more safely predicted by the Monte Carlo simulation. A total relative uncertainty of 40% is finally quoted for the $q\bar{q}$ contamination in the inclusive sample, yielding a 2.9% relative uncertainty on the branching ratio. The effect due to the $q\bar{q}$ background is much reduced in the exclusive modes because of the hadronic mass cut and the track multiplicity requirement.

In the $K_S^0 K_S^0 \pi^- \nu_\tau$ channel, the Monte Carlo predicts no background event inside the chosen mass window, with an uncertainty of 0.2 event; this translates into a 3.3% systematic uncertainty in the evaluation of the branching ratio. The dominant background for $K_S^0 h^+ h^- h^- \nu_\tau$ is the $K_S^0 K_S^0 \pi^- \nu_\tau$ channel, in which both K_S^0's decay into $\pi^+ \pi^-$, introducing a 19% uncertainty. For the $K_S^0 \pi^- \pi^0 \pi^0 \nu_\tau$ channels, the backgrounds are mainly from the combinatorial background, the $K_S^0 \pi^- \pi^0$ mode and the $K_S^0 K_S^0 \pi^-$ mode with one K_S^0 decaying into two π^0's, giving a 8.8% uncertainty for $K_S^0 \pi^- \pi^0 \pi^0 \nu_\tau$.

Since K_S^0's can be produced via nuclear interactions on the detector material, this effect is also investigated. The Monte Carlo predicts about 1% of K_S^0's in the inclusive mode produced in this way. To check this effect between data and Monte Carlo, the numbers of primary charged hadrons and the secondary charged hadrons are required to be one and at least three, in order to emphasize the K_S^0's from nuclear interactions (yielding additional charged tracks) with respect to the primary ones. The agreement allows to assign a systematic uncertainty of 2% on the inclusive branching ratio for this effect.

Finally, fake K_S^0's due to nuclear interactions are also investigated for the $K_S^0 h^- h^+ h^-$ and $K_S^0 h^- \pi^0 \pi^0$ modes. In these two modes, low statistics forbids the separation of the signal from mass combinations accidentally falling into the K_S^0 mass window. Since these fake K_S^0's are mostly produced at the positions of the ITC and TPC walls, the study of the L_{xy} distribution gives a chance to address this effect. The K_S^0 candidates in data are consistent with an exponential shape in the L_{xy} distribution and an uncertainty of 10% is assigned to both $K_S^0 h^- h^+ h^-$ and $K_S^0 h^- \pi^0 \pi^0$ modes.

9.6   Monte Carlo statistics and dynamics

The uncertainties due to Monte Carlo statistics are estimated using the errors given in Table 2. The dynamics of the decays can also affect the efficiencies, because of the momentum dependence of the K_S^0 acceptance shown in Fig. 4. In the measurement of the inclusive mode, the analysis in momentum slices minimizes the effect of uncertainties in dynamics. The remaining uncertainty due to the bin width is estimated by computing the deviation from data in each momentum slice, yielding a 1.2% uncertainty.

The dynamics of the $K_S^0 \pi^-$ mode is dominated by $K^{*-}(892)$ production. Since

some small discrepancies are observed in the mass spectrum (see Section 10.1), a 0.4% uncertainty is estimated from the study of the slight mass dependence of the efficiency. For the $K^0_S K^-$ mode, the model [7] used in the simulation assumes this decay proceeds through the high energy tail of the $\rho(770)$. However, data show a $(+100 \pm 35)$ MeV/c^2 shift in the hadronic mass distribution of these decays, compared to the prediction of this model. The efficiencies in Table 2 reflect a relative +8.8% correction for this shift; the uncertainty due to this correction brings about a 4.7% error for this decay mode. In addition, the dynamics can also affect the $x_\pi(K)$ parameters through the track overlap. A 1.9% uncertainty is estimated by varying the mean of the invariant hadronic mass and observing the change in the $x_\pi(K)$ parameters.

For the $K^0 h \pi^0$ modes, the decay dynamics not only affect the K^0_S momentum, but also the π^0 momentum distributions. By examining the efficiency variation as a function of the total invariant mass, one can estimate the systematic uncertainties corresponding to possible mass shifts, which depend on the relevant dynamics for the $K\pi\pi$ and $KK\pi$ modes. In view of isospin invariance, one can directly use the result of the total invariant mass study in the purely charged modes [9], in which total hadronic mass corrections for both decay modes are applied. The corrected efficiencies are listed in Table 2 and the variation of efficiencies due to the corrections are treated as the systematic uncertainties, which are estimated to be 6.3% for $K^0_S \pi^- \pi^0$, 5.0% for $K^0_S K^- \pi^0$ and 6.0% for $K^0_S K^0_S \pi^-$. The shape of the δ_E distribution for the events with a K^0_L component depends on the distribution of the K^0_L momentum. For $K^0_S K^0_L \pi^-$, the dynamics should be the same as for $K^- K^+ \pi^-$, which is investigated in Ref. [9]. In the $K^- K^+ \pi^-$ mode, the uncertainty on the mean kaon momentum is 1 GeV/c, corresponding to an uncertainty of 0.15 on δ_E. By shifting the mean of δ_E by this amount for the K^0_L shape and repeating the procedure used for fitting the K^0_L component, a 5.6% of uncertainty is estimated for the $K^0_S K^0_L \pi^-$ channel. Since $B(\tau^- \to K^0_S K^- \pi^0 \nu_\tau)$ involves the dE/dx measurement, a 1.7% is estimated for $K^0_S K^- \pi^0$, accounting for the effect of unknown dynamics in the determination of the x_π parameters.

Finally, a 10% relative uncertainty is assigned to each of the channels producing a K^0_S and three hadrons, for which the efficiencies are estimated by means of a phase-space generator. However the limited available phase space in these decays is the dominant effect on their efficiencies. An additional uncertainty of 15% is introduced for the $K^0 h^+ h^- h^-$ mode to take into account the unknown composition of the final state.

10 Investigation of mass spectra

The mass spectra in the $K^0_S h^-$ and $K^0_S h^- \pi^0$ modes are investigated in this section. For this purpose, samples are selected with the K^0_S mass windows used in the analysis of $K^0_S K^- (\pi^0)$ and $K^0_S K^0_L \pi^- (\pi^0)$ decays. Setting a cut on the x_π variable allows one to partially separate the states with accompanying charged kaons from those with charged pions. Similarly, a minimum requirement on δ_E enhances the channels containing a K^0_L.
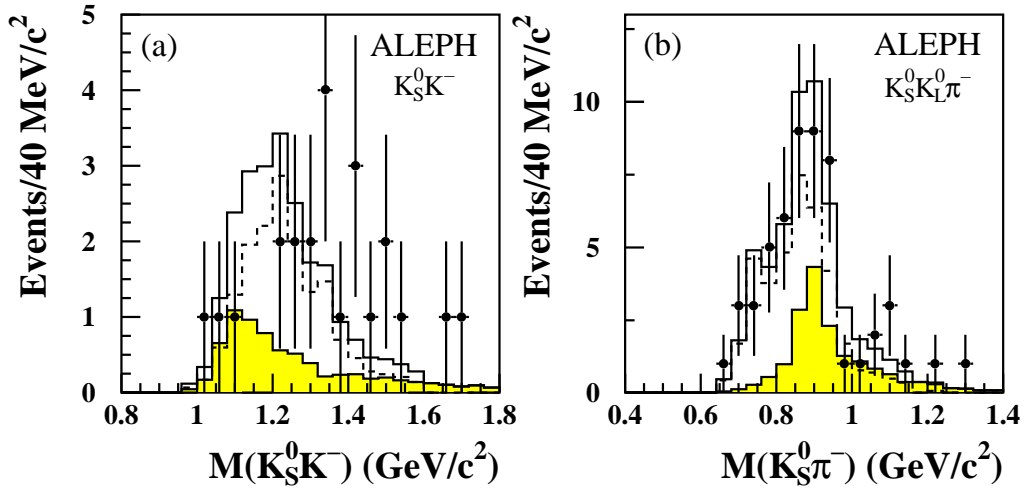
Figure 8: *Invariant mass distributions of (a) $K^0_S K^-$ for the selected $\tau^- \to K^0_S K^- \nu_\tau$ events and (b) $K^0_S \pi^-$ for the selected $\tau^- \to K^0_S K^0_L \pi^- \nu_\tau$ are shown for data (points with error bars) and for Monte Carlo prediction (open histograms). The backgrounds are given in the shaded histograms and the model predictions [6, 7] are indicated by the dashed lines.*

10.1 Mass spectra in the $K^0_S h^-$ sample

The decay $\tau^- \to K^0_S K^- \nu_\tau$ is selected from the $K^0_S h^-$ sample by requiring $x_\pi \leq -2$ and $p_K \geq 5$ GeV/c, yielding a purity of about 70%. Backgrounds mostly contaminate the low mass region, as shown in Fig. 8; from the same figure one can see that the observed $K^0_S K$ invariant mass distribution does not agree with the predictions based on the $\rho \to K\bar{K}$ model [7]. A significant shift of the mean value of the Monte Carlo distribution is observed, resulting in a systematic effect discussed in Section 9.6.

The decay $\tau^- \to K^0_S K^0_L \pi^- \nu_\tau$ can also be selected by requiring $\delta_E \geq 2$, enhancing the signal up to about 70% purity. The corresponding $K^0_S \pi^-$ invariant mass spectrum is also shown in Fig. 8. A $K^{*-}(892)$ signal is observed. However, after subtraction of the contribution from $K^0_S \pi^-$, the statistics of the data does not allow a conclusion to be drawn on the dominance of $K^{*-}(892)$ in the $K^0_S K^0_L \pi^-$ mode, in which a $K^{*-}(892)$ can be formed either by $K^0_S \pi^-$ or $K^0_L \pi^-$.

The $K^0_S \pi^-$ mass spectrum for the complete $K^0_S h^- \nu_\tau$ sample, assuming the primary hadron to be a pion, is shown in Fig. 9. The contributions of $K^0_S K^- \nu_\tau$ and $K^0_S K^0_L \pi^- \nu_\tau$ are also given, together with the combinatorial background. The $K^{*-}(892)$ dominance is clearly seen. The combinatorial background yields a rather flat mass distribution while $K^0_S K^- \nu_\tau$ affects the higher mass region. A small mass shift is seen comparing to the expected $K^{*-}(892)$ peak. Some excess at large masses is also observed and a systematic uncertainty on the branching ratio is estimated accordingly in Section 9.6. The possible

contribution of higher K^*'s cannot be extracted in view of the limited statistics.

10.2 Mass spectra in the $K_S^0 h^- \pi^0$ sample

Because of the limited statistics, the channels involving charged kaons cannot be studied in this analysis. The invariant mass spectra are investigated by requiring $p_{K_S^0} > 5$ GeV$/c$ and assuming the accompanying primary charged particle to be a pion (see Fig. 10). A 53% purity for the $K_S^0 \pi^- \pi^0$ signal can be achieved. The main expected contributions are from $K_S^0 K^- \pi^0$, $\overline{K}^0 K^0 \pi^-$ and $\overline{K}^0 K^0 \pi^- \pi^0$, amounting to 18%, 10% and 8% of the total selected sample, respectively. No evident $K^{*-}(892)$ signal appears in the $K_S^0 \pi^-$ invariant mass spectrum, indicating the suppression of the $K^{*-}\pi^0$ intermediate state in $\tau^- \to \overline{K}^0 \pi^- \pi^0 \nu_\tau$. An obvious discrepancy between data and the model prediction [6] is observed in the $K_S^0 \pi^0$ invariant mass: data show a $K^{*0}(892)$ signal. It is not clear if this $K^{*0}(892)$ comes from the $\overline{K}^0 \pi^- \pi^0 \nu_\tau$ or the $K^0 K^- \pi^0 \nu_\tau$ channel, although the dE/dx information for the charged hadrons favours the latter situation, in disagreement with the model [6] used in the Monte Carlo simulation. This spectrum is thus not well suited to fit a $K^{*0}(892)$ fraction in the $\overline{K}^0 \pi^- \pi^0 \nu_\tau$ final state. On the contrary, it is easier to interpret the $\pi^- \pi^0$ mass spectrum where a clear ρ signal is seen, while the backgrounds are found mostly in the low $\pi^- \pi^0$ mass region. Therefore the uncertainty on the background is reduced in the ρ region and the fit of this distribution in terms of ρ and K^* components is more reliable. The determination of the ρK fraction follows the method used in the $K^- \pi^+ \pi^- \nu_\tau$ channel [9]. Backgrounds are subtracted according to their branching ratios and the relevant efficiencies. The final $\pi^- \pi^0$ invariant mass spectrum is fitted with an incoherent sum of a ρ Breit-Wigner signal and the shape of the $K^* \pi$ reflections obtained from the simulation. The $\overline{K}^0 \rho^-$ fraction is found to be $(64 \pm 9 \pm 10)\%$ (see Fig. 11), where the last error accounts for the uncertainty on the shape of the mass spectrum from both $\overline{K}^0 K^0 \pi^-$ and $K^0 K^- \pi^0$. The obtained fraction implies a significant $K_1(1270)$ contribution in the decay $\tau^- \to \overline{K}^0 \pi^- \pi^0 \nu_\tau$, since $K_1(1400)$ dominantly decays via $K^* \pi$, unlike $K_1(1270)$.

Finally, the $K_S^0 \pi^- \pi^0$ invariant mass distribution is also investigated in Fig. 10(d), showing a rather broad structure around 1.3 GeV$/c^2$. This distribution looks similar to the three-prong case [9], indicating both $K_1(1270)$ and $K_1(1400)$ contributions to the $\overline{K}^0 \pi^- \pi^0 \nu_\tau$ decay, unlike the model used in the Monte Carlo generator.

11 Results and discussion

The branching ratios measured by the present analysis are summarized in Table 8. The sum of all exclusive branching ratios with K_S^0's is equal to $(9.28 \pm 0.65 \pm 0.54) \times 10^{-3}$, which is in agreement with the inclusive measurement $(9.70 \pm 0.58 \pm 0.62) \times 10^{-3}$. The difference between these two results, $\Delta B = (0.42 \pm 0.21 \pm 0.41) \times 10^{-3}$, where the uncertainties take into account only the uncommon statistics and systematics, leaves little room for the presence of other significant exclusive modes with K_S^0's.

The results for the modes with one K^0 are in good agreement with other published
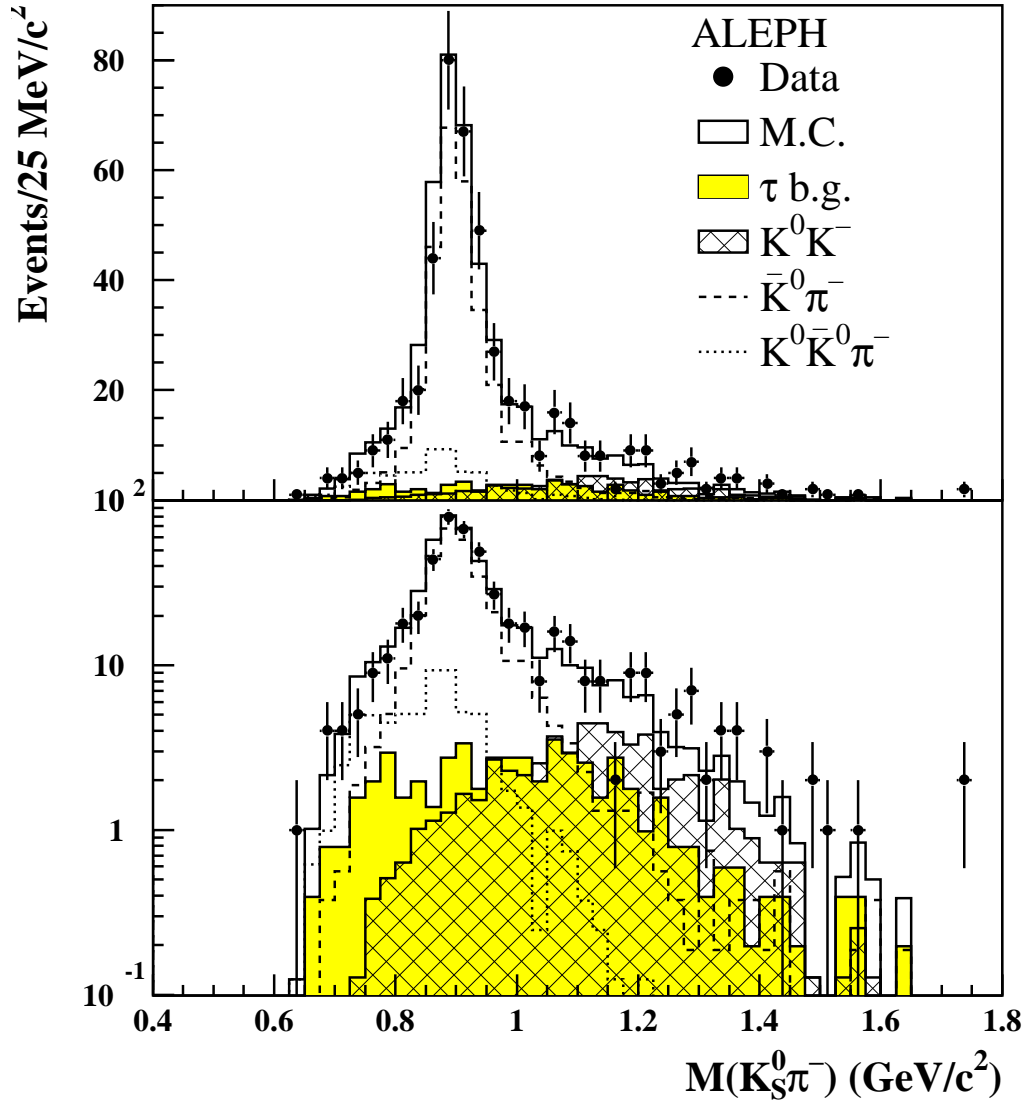
Figure 9: *Invariant mass distribution of $K_S^0\pi^-$ candidates in the $K_S^0 h^-$ sample for data (points with error bars) and Monte Carlo prediction (open histograms) [6, 7], respectively. The signal and τ background contributions are also shown.*
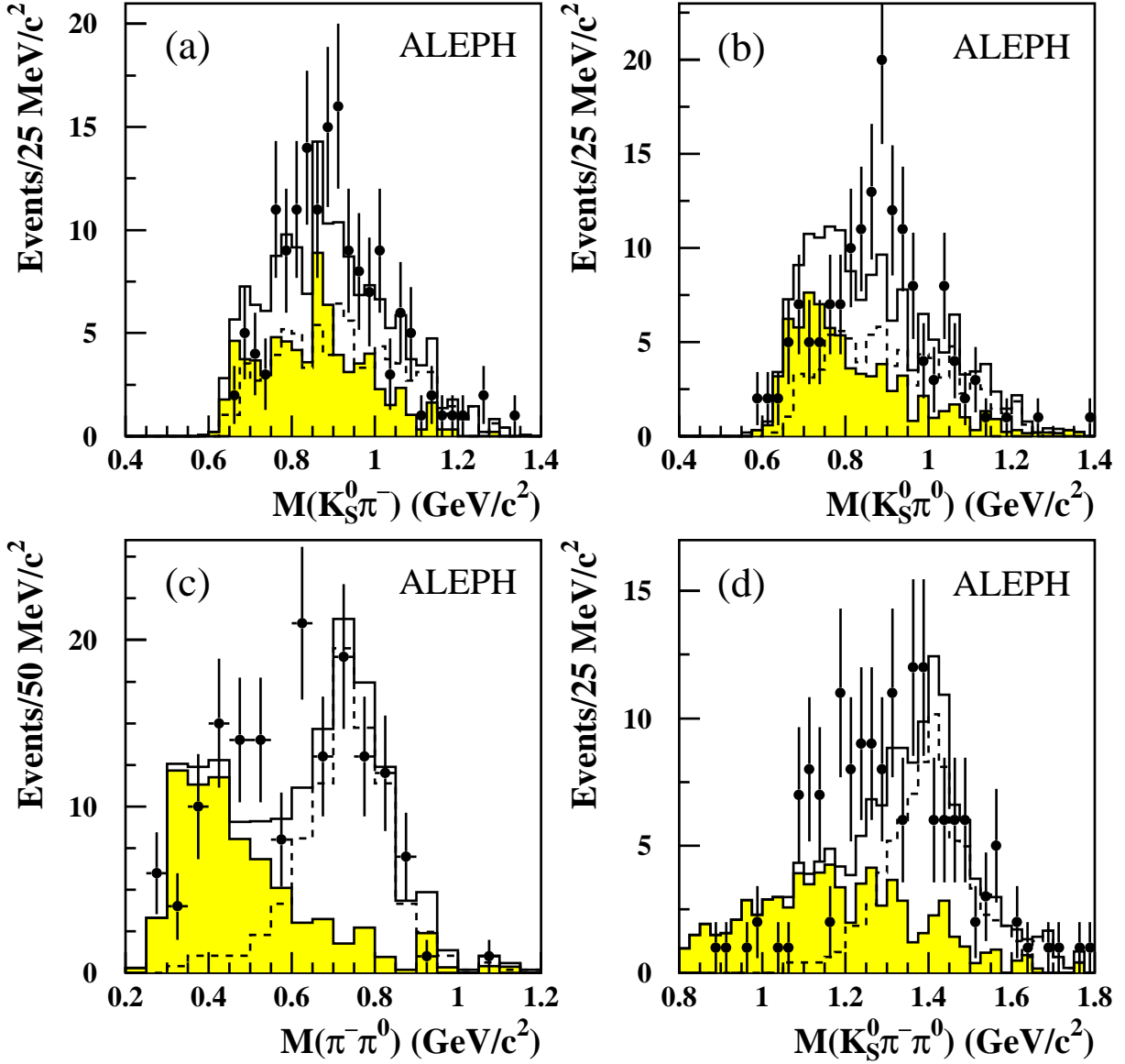
Figure 10: *Invariant mass distributions of (a) $K_S^0 \pi^-$, (b) $K_S^0 \pi^0$, (c) $\pi^- \pi^0$ and (d) $K_S^0 \pi^- \pi^0$ for $\tau^- \to K^0 h^- \pi^0 \nu_\tau$. Data (points with error bars), Monte Carlo predictions (open histograms) and background contributions (shaded histograms) are shown. Also shown are the model expectation [6] for the $K^0 \pi^- \pi^0 \nu_\tau$ decay (dashed histograms).*
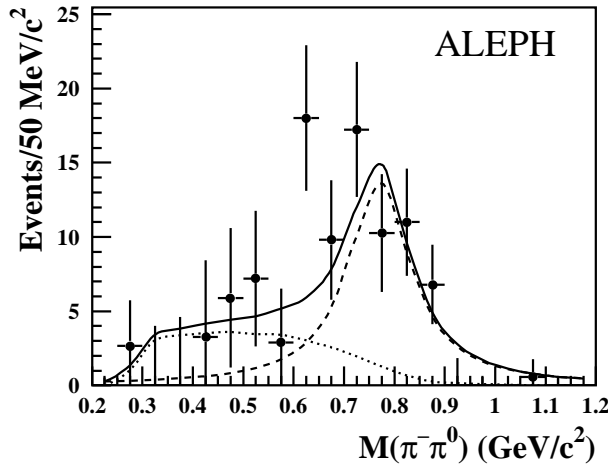
24

Figure 11: *The $\pi^-\pi^0$ invariant mass after background subtraction in the decay $\tau^- \to K_S^0\pi^-\pi^0\nu_\tau$, where the fit (solid curve) is a sum of the ρ Breit-Wigner form (dashed) and the expected shape of the $K^*\pi$ reflection (dotted).*

results [1, 14, 15], as shown in Fig. 12. The relevant exclusive modes are added, yielding

$$B(\tau^- \to K^0 h^- \nu_\tau) = (1.01 \pm 0.11 \pm 0.07)\%, \tag{17}$$

and

$$B(\tau^- \to K^0 h^- \pi^0 \nu_\tau) = (4.46 \pm 0.52 \pm 0.46) \times 10^{-3}. \tag{18}$$

where the correlation between the exclusive modes are taken into account.

The decay $\tau^- \to \overline{K}^0 K^0 \pi^- \nu_\tau$ is also investigated by studying both $\tau^- \to K_S^0 K_L^0 \pi^- \nu_\tau$ and $\tau^- \to K_S^0 K_S^0 \pi^- \nu_\tau$. The first mode is determined for the first time and is observed to dominate the $\overline{K}^0 K^0 \pi^- \nu_\tau$ channel. For the second mode, a recent CLEO measurement gives $B(\tau^- \to K_S^0 K_S^0 \pi^- \nu_\tau) = (0.23 \pm 0.05 \pm 0.03) \times 10^{-3}$ [14], which is about four standard deviations lower than the prediction of [7]. The value obtained in the present analysis, $B(\tau^- \to K_S^0 K_S^0 \pi^- \nu_\tau) = (0.26 \pm 0.10 \pm 0.05) \times 10^{-3}$ agrees with the CLEO measurement and confirms the trend. Because $B(\tau^- \to K_S^0 K_S^0 \pi^- \nu_\tau) = B(\tau^- \to K_L^0 K_L^0 \pi^- \nu_\tau)$, a direct measurement of the branching ratio for $\tau^- \to \overline{K}^0 K^0 \pi^- \nu_\tau$ is achieved:

$$B(\tau^- \to \overline{K}^0 K^0 \pi^- \nu_\tau) = (1.53 \pm 0.30 \pm 0.16) \times 10^{-3}. \tag{19}$$

This value agrees with that obtained for the charged mode $B(\tau^- \to K^- K^+ \pi^- \nu_\tau) = (1.67 \pm 0.21 \pm 0.16) \times 10^{-3}$ [9], as expected from isospin symmetry in the absence of second-class currents [16].

The $\overline{K}^0 \rho^-$ fraction in the decay $\tau^- \to \overline{K}^0 \pi^- \pi^0 \nu_\tau$ is determined to be $(64 \pm 9 \pm 10)\%$. Assuming that this channel proceeds only via an incoherent superposition of the intermediate states $K\rho$ and $K^*\pi$, one obtains

$$B(\tau^- \to (\overline{K}^*\pi)^- \nu_\tau \to \overline{K}^0 \pi^- \pi^0 \nu_\tau) = (1.06 \pm 0.37 \pm 0.32) \times 10^{-3}, \tag{20}$$

25

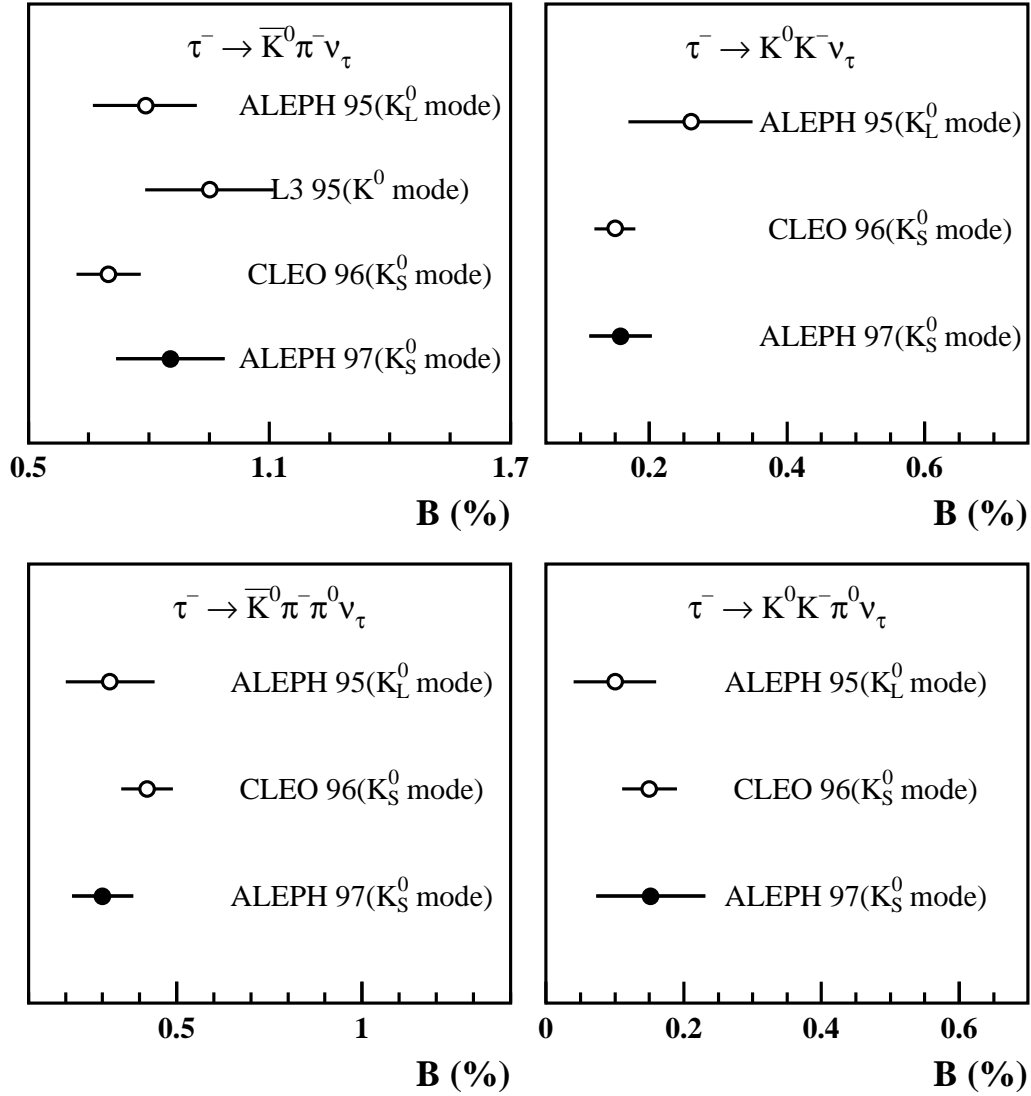Figure 12: *The published branching ratios for $\tau^- \to \overline{K}^0 \pi^- (\pi^0) \nu_\tau$ and $\tau^- \to K^0 K^- (\pi^0) \nu_\tau$. The black dots correspond to this analysis. The detected K^0 modes are given in parentheses for each experiment.*

Mode	B (10^{-3})
$K_S^0 X^- \nu_\tau$	$9.70 \pm 0.58 \pm 0.62$
$\overline{K}^0 \pi^- \nu_\tau$	$8.55 \pm 1.17 \pm 0.66$
$\overline{K}^0 \pi^- \pi^0 \nu_\tau$	$2.94 \pm 0.73 \pm 0.37$
$K^0 K^- \nu_\tau$	$1.58 \pm 0.42 \pm 0.17$
$K^0 K^- \pi^0 \nu_\tau$	$1.52 \pm 0.76 \pm 0.21$
$K_S^0 K_L^0 \pi^- \nu_\tau$	$1.01 \pm 0.23 \pm 0.13$
$K_S^0 K_L^0 \pi^- \pi^0 \nu_\tau$	$0.31 \pm 0.11 \pm 0.05$
$K_S^0 K_S^0 \pi^- \nu_\tau$	$0.26 \pm 0.10 \pm 0.05$
$K_S^0 K_S^0 \pi^- \pi^0 \nu_\tau$	< 0.20 (95% C.L.)
$\overline{K}^0 \pi^- \pi^0 \pi^0 \nu_\tau$	$0.58 \pm 0.33 \pm 0.14$
$K^0 K^- \pi^0 \pi^0 \nu_\tau$	< 0.39 (95% C.L.)
$K^0 h^+ h^- h^- \nu_\tau$	$0.23 \pm 0.19 \pm 0.07$

Table 8: Summary of branching ratios obtained in this analysis.

and

$$B(\tau^- \to \overline{K}^0 \rho^- \nu_\tau \to \overline{K}^0 \pi^- \pi^0 \nu_\tau) = (1.88 \pm 0.54 \pm 0.38) \times 10^{-3}. \tag{21}$$

The physics implications of the present results will be discussed in a subsequent paper, where the recently published results on three-prong τ decays with charged kaons [9] and the forthcoming ALEPH measurements of charged kaons and K_L^0's in one-prong τ decays will be also taken into account.

12   Conclusion

The branching ratios for τ decays involving K_S^0's with up to three accompanying hadrons in the final states are measured. A first measurement of the branching ratio for the decay $\tau^- \to K_S^0 K_L^0 \pi^- \nu_\tau$ is achieved, which together with the determination of $\tau^- \to K_S^0 K_S^0 \pi^- \nu_\tau$ separates the different contributions to the $\tau^- \to \overline{K}^0 K^0 \pi^- \nu_\tau$ decay. By exploiting the dE/dx measurement, exclusive decay modes with a charged kaon or pion are extracted. The results are summarized in Table 8. The measurements which can be compared to published values are displayed in Fig. 12, showing agreement.

Acknowledgements

References

[1] ALEPH Collaboration, *Tau hadronic branching ratios*, Z. Phys. C70 (1996) 579.

[2] R.M. Barnett et al. Particle Data Group, Phys. Rev. D54 (1996) 1.

[3] M. Davier, "τ decays into strange particles and QCD", *Proceedings of "The Fourth International Workshop on Tau physics", September 1996, Estes Park, Colorado, USA*. Published in Nucl. Phys. Proc. Suppl. 55C, 395(1997).

[4] M. Suzuki, Phys. Rev. D47 (1993) 1252.

[5] J.J. Gomez-Cadenas, M.C. Gonzalez-Garcia, A. Pich, Phys. Rev. D42 (1990) 3093.

[6] R. Decker, E. Mirkes, R. Sauer, Z. Was, Z. Phys. C58 (1993) 445.

[7] M. Finkemeier, E. Mirkes, Z. Phys. C69 (1996) 243.

[8] B.A. Li, Phys. Rev. D55 (1997) 1436.

[9] ALEPH Collaboration, *Three-prong tau decays with charged kaons*, CERN-PPE/97-069, to appear in European Physics Journal C.

[10] ALEPH Collaboration, *ALEPH: a detector for electron-positron annihilations at LEP*, Nucl. Inst. Methods A294 (1990) 121;
ALEPH Collaboration, *Performance of the ALEPH detector at LEP*, Nucl. Inst. Methods A360 (1995) 481.

[11] KORALZ, S. Jadach, B.F.L. Ward, Z. Was. Comp. Phys. Comm. 66 (1991) 276; 79 (1994) 503; TAUOLA, S. Jadach, Z. Was, R. Decker, J.H. Kuhn, Comp. Phys. Comm. 76 (1993) 361.

[12] T. Sjöstrand, Comp. Phys. Comm. 82 (1994) 74.

[13] ALEPH Collaboration, *Tau leptonic branching ratios*, Z. Phys. C70 (1996) 561.

[14] CLEO Collaboration, *Decays of tau leptons to final states containing K_S^0 mesons*, Phys. Rev. D53 (1996) 6037.

[15] L3 Collaboration, *One prong tau decays with neutral kaons*, Phys. Lett. B352 (1995) 487.

[16] A. Rougé, Z. Phys. C70 (1996) 65.